AGU PUBLICATIONS

JGR

Journal of Geophysical Research: Earth Surface

RESEARCH ARTICLE
10.1002/2016JF003965

Key Points:
- We develop a Lagrangian model of bed material sediment transport and in-channel storage dynamics on a river network
- Pulsing the system with Poisson sediment arrivals allows for analytical insight on bed sediment dynamics
- Emergence of low-transport capacity reaches creates "bottlenecks" which dynamically alter the downstream sediment supply

Interplay between spatially explicit sediment sourcing, hierarchical river-network structure, and in-channel bed material sediment transport and storage dynamics

Jonathan A. Czuba[1,2], Efi Foufoula-Georgiou[3], Karen B. Gran[4], Patrick Belmont[5], and Peter R. Wilcock[5]

[1]Department of Civil, Environmental, and Geo-Engineering, St. Anthony Falls Laboratory, and Institute on the Environment, University of Minnesota, Twin Cities, Minneapolis, Minnesota, USA, [2]Now at the Department of Earth and Atmospheric Sciences, Indiana University, Bloomington, Indiana, USA, [3]Department of Civil and Environmental Engineering, University of California, Irvine, California, USA, [4]Department of Earth and Environmental Sciences, University of Minnesota, Duluth, Minnesota, USA, [5]Department of Watershed Sciences, Utah State University, Logan, Utah, USA

Correspondence to:
J. A. Czuba,
jczuba@indiana.edu

Citation:
Czuba, J. A., E. Foufoula-Georgiou, K. B. Gran, P. Belmont, and P. R. Wilcock (2017), Interplay between spatially explicit sediment sourcing, hierarchical river-network structure, and in-channel bed material sediment transport and storage dynamics, *J. Geophys. Res. Earth Surf.*, *122*, 1090–1120, doi:10.1002/2016JF003965.

Received 18 MAY 2016
Accepted 8 APR 2017
Accepted article online 18 APR 2017
Published online 9 MAY 2017

Abstract Understanding how sediment moves along source to sink pathways through watersheds—from hillslopes to channels and in and out of floodplains—is a fundamental problem in geomorphology. We contribute to advancing this understanding by modeling the transport and in-channel storage dynamics of bed material sediment on a river network over a 600 year time period. Specifically, we present spatiotemporal changes in bed sediment thickness along an entire river network to elucidate how river networks organize and process sediment supply. We apply our model to sand transport in the agricultural Greater Blue Earth River Basin in Minnesota. By casting the arrival of sediment to links of the network as a Poisson process, we derive analytically (under supply-limited conditions) the time-averaged probability distribution function of bed sediment thickness for each link of the river network for any spatial distribution of inputs. Under transport-limited conditions, the analytical assumptions of the Poisson arrival process are violated (due to in-channel storage dynamics) where we find large fluctuations and periodicity in the time series of bed sediment thickness. The time series of bed sediment thickness is the result of dynamics on a network in propagating, altering, and amalgamating sediment inputs in sometimes unexpected ways. One key insight gleaned from the model is that there can be a small fraction of reaches with relatively low-transport capacity within a nonequilibrium river network acting as "bottlenecks" that control sediment to downstream reaches, whereby fluctuations in bed elevation can dissociate from signals in sediment supply.

1. Introduction

Erosion of near-channel sediment sources now dominates the sediment load in many agricultural landscapes [*Belmont et al.*, 2011; *Massoudieh et al.*, 2013; *Kronvang et al.*, 2013; *Neal and Anders*, 2015]. This finding comes from a number of studies employing a variety of approaches including bed load and suspended load monitoring, setting bank-erosion pins, aerial photograph analysis, and sediment fingerprinting. Also, this finding has been observed in a wide range of environments including the rapidly incising Le Sueur River in southern Minnesota (2880 km^2, 78% of basin in agriculture, and 70% of sediment supply from near-channel erosion of bluffs, banks, and ravines) [*Belmont et al.*, 2011], the legacy-sediment laden Mill Stream, a tributary of the Chesapeake Bay in Maryland (32 km^2, 74% agriculture, and 83–99% of sediment supply from bank erosion) [*Massoudieh et al.*, 2013], the River Odense in Denmark (486 km^2, 71% agriculture, and 90–94% of sediment supply from bank erosion) [*Kronvang et al.*, 2013], and Wildcat Slough in central Illinois (61 km^2, 99% agriculture, and 40–65% of sediment supply from bank erosion) [*Neal and Anders*, 2015]. The finding that near-channel sediment sources often dominate may be surprising as sediment generated in agricultural landscapes has historically been primarily sourced from upland fields [*Trimble*, 1981, 1983; *Belmont et al.*, 2011]. At least in the Le Sueur River Basin, an expansion and intensification of agricultural drainage has both decreased surface runoff and erosion and increased crop yields but at the expense of delivering more water to ditches, streams, and rivers than in the past, resulting in amplified streamflows and more erosive rivers [*Blann et al.*, 2009; *Belmont et al.*, 2011; *Schottler et al.*, 2014; *Foufoula-Georgiou et al.*, 2015].

As near-channel sediment sources become increasingly recognized as dominant in modern agricultural landscapes, the modeling frameworks used to simulate sediment transport at the watershed scale must also undergo a shift. Watershed-scale, sediment-transport models applied to agricultural landscapes have conventionally assumed that upland soil erosion is the dominant sediment source. Such models estimate upland soil erosion using the universal soil loss equation [*Renard et al*., 1997] and apply a sediment-delivery ratio to estimate watershed sediment yield (e.g., HSPF [see *Shenk and Linker*, 2013] and SWAT [see *Gassman et al*., 2007]). While efforts have been made to incorporate near-channel sediment sources into these models, representation of sediment-transport processes remains nascent.

However, a few network-based modeling frameworks exist that can easily incorporate near-channel sediment sources [*Benda and Dunne*, 1997a; *Jacobson and Gran*, 1999; *Wilkinson et al*., 2006; *Czuba and Foufoula-Georgiou*, 2014, 2015; *Schmitt et al*., 2016; *Gran and Czuba*, 2017]. The seminal work is that of *Benda and Dunne* [1997a] where stochastically forced sediment inputs were routed through a 215 km^2 river network in the Oregon Coast Range via a sediment mass-balance approach. Distributed inputs to their network model included (1) landslides, debris flows, and fluvial scour from bedrock hollows in first- and second-order channels; (2) soil creep along the toe of hillslopes; (3) landslides from bedrock hollows that laterally enter a stream reach; and (4) bank erosion of debris-flow fans and terraces. *Jacobson and Gran* [1999] developed a simple network routing model of the 5200 km^2 Current River Basin in the Ozarks of Missouri to explain how gravel inputs delivered to first-order channels and subsequently routed through the network could explain the spatial distribution of gravel bars. *Wilkinson et al.* [2006] computed the spatial distribution of bed material sediment accumulation in the 29,000 km^2 Murrumbidgee River Basin in southeast Australia by comparing the total bed material sediment supply from gullies, river banks, and upstream tributaries against the sediment-transport capacity in each reach.

More recently, the network-based framework of *Czuba and Foufoula-Georgiou* [2014, 2015] was used to route sand-sized sediment through the channel network of the 44,000 km^2 Minnesota River Basin (or a subbasin: the 9200 km^2 Greater Blue Earth River Basin) in southern Minnesota. Their framework introduced theoretically derived, sand-transport time delays that were specified as a function of position in the network (e.g., upstream drainage area) and local channel characteristics (e.g., channel slope and grain size). While developments are still ongoing, this framework has the potential to incorporate any type of sediment input along the river network as well as storage processes. *Gran and Czuba* [2017] incorporated a sediment budget of the Greater Blue Earth River Basin [*Bevis*, 2015] along with an in-channel storage process into the network-based framework of *Czuba and Foufoula-Georgiou* [2014, 2015] primarily to assess how sediment pulses (in excess of a background supply) are affected by river-network structure. Additionally, the network-based CASCADE (CAtchment Sediment Connectivity And DElivery) modeling framework of *Schmitt et al.* [2016] identifies sediment cascades which show how a specific source is connected to its multiple sinks. The CASCADE model was applied to the 51,000 km^2 Da River Basin within Vietnam, China, and Laos to quantitatively analyze the sediment connectivity of the basin. The work of *Schmitt et al.* [2016] provides some important new developments for network-based, sediment-transport models including the specification of the full grain-size distribution of bed material sediment and adding competition functions for determining which grain sizes to transport in a given reach.

With the availability of detailed topography from lidar data, we can accurately map the sources of sediment and pathways by which sediment moves through a watershed [*Passalacqua et al*., 2012, 2015]. In some basins, this may reveal a strong heterogeneous potential for sediment generation (e.g., location of bluffs and ravines). Paired with repeat field measurements or geochemical sediment fingerprinting, this allows one to quantify the magnitude and frequency of sediment generation for features identified on the landscape [*Day et al*., 2013a; *Stout et al*., 2014; *Schaffrath et al*., 2015]. Furthermore, physical characteristics of the channels (e.g., slope and width) can be extracted from detailed topography [e.g., *Tarboton et al*., 1991] to compute the rate of sediment movement through, and transport capacity of, various reaches. This is the essence of network-based, sediment-transport models which have the potential to explore synchronizations of sediment delivery [*Czuba and Foufoula-Georgiou*, 2014], emergence of hot spots of geomorphic change [*Czuba and Foufoula-Georgiou*, 2015], and also test alternative scenarios for management decisions.

The purpose of this paper is to develop a bed material sediment routing model that combines spatially explicit sediment sourcing with in-channel transport and storage dynamics on a river network (Figure 1) within the framework of *Czuba and Foufoula-Georgiou* [2014, 2015]. The model is able to compute spatiotemporal

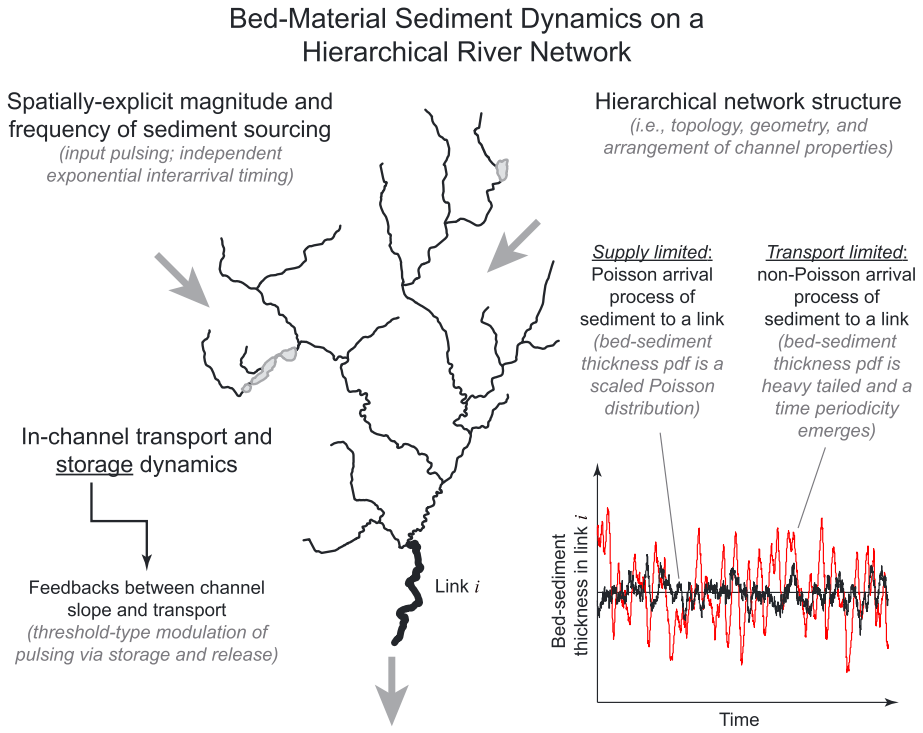

Figure 1. Conceptual overview of bed material sediment dynamics on a hierarchical river network. The combination of spatially explicit magnitude and frequency of sediment sourcing, hierarchal network structure, and in-channel transport and storage dynamics creates a temporal variability in bed sediment thickness. Under supply-limited conditions, the bed sediment thickness probability distribution function (pdf) is a scaled Poisson distribution, which is directly related to the Poisson arrival structure of the inputs. Under transport-limited conditions, the bed sediment thickness pdf is heavy tailed and the temporal dynamics exhibit a characteristic timescale (periodicity).

changes in bed sediment thickness along an entire river network, elucidating how river networks organize and process sediment supply. The bed sediment thickness that we present herein is a theoretical quantity that represents the amount of sediment on top of a nonerodible surface that we assumed to be located near the existing bed. We apply our model to sand transport in the agricultural Greater Blue Earth River Basin in Minnesota. The arrival of sediment to links of the network is cast as a Poisson process, and the model is used to simulate transport and storage dynamics over a 600 year time period. Properties of the Poisson arrival process allow us to derive analytically (under supply-limited conditions) the time-averaged probability distribution function (pdf) of bed sediment thickness for each link of the river network for any spatial distribution of inputs. Under transport-limited conditions, the assumptions of the Poisson arrival process are violated due to in-channel storage dynamics that preclude an analytical derivation of the pdf of bed sediment thickness. Instead, we are able to (1) compute semianalytically the time-averaged bed sediment thickness and (2) provide a lower limit on the temporal variability of bed sediment thickness. This is accomplished by computing iteratively the bed slope adjustment required to pass the sediment supply, converting it to bed sediment thickness, and then adding this to the analytically derived bed sediment thickness under supply-limited conditions. We use the discrepancy in the temporal variability of bed sediment thickness between our semianalytical estimates and model simulations to isolate the influence of, and obtain key insights into, river-network structure on bed material sediment dynamics.

2. Network-Based Modeling Framework for Bed Material Sediment

The network-based modeling framework described by *Czuba and Foufoula-Georgiou* [2014] is a first-order approach to understanding the transport dynamics of an environmental flux (e.g., sediment, nitrogen, and phosphorous) along a network by combining system connectivity with major transport and transformation processes (e.g., advection, removal of nitrate through denitrification, and transformation of phosphorous between dissolved and particulate forms). As applied to bed material sediment herein, the result is a

Lagrangian transport model of sediment through a river network (section 2.1) where sediment is supplied in space and time (section 2.2), transported downstream via physically based time delays (section 2.3), and stored in channel whenever transport capacity is exceeded (section 2.4). The resulting model of bed material sediment lends itself to some analytical insights that are described in section 2.5. Basic elements of the model are described in this section; further details regarding the application of the model to the study basin are described in section 3.

2.1. Network of Connected Flow paths

A network of connected flow paths forms the basis of the model. Herein, we focus on a river network, derived from a digital elevation model (DEM) [e.g., *Tarboton et al*., 1991; *Passalacqua et al*., 2010] that is conceptualized as a set of connected links. Each link *i* represents either a segment of river channel between tributaries and/or lakes or a lake that intersects the river network. Each link is associated with a set of unique topologic, physical, and hydrodynamic attributes. For instance, a river channel would have the following attributes: index of link *i*, index of upstream and downstream links, link length ℓ_i [L], directly contributing area a_i [L^2] (i.e., the incremental area that drains directly to link *i*), upstream drainage area A_i [L^2] (i.e., the sum of a_i for all links upstream of and including link *i*), elevation of the bed at the upstream end of the link $\eta_{i,t}$ [L], and channel slope $S_{i,t}$; herein, both $\eta_{i,t}$ and $S_{i,t}$ vary in time and thus include a subscript *t*. Additional attributes associated with transport and storage dynamics can be computed from or parameterized by these attributes (see sections 2.3, 2.4, and 3.4).

2.2. Spatial and Temporal Supply

An individual sediment input to the network is referred to as a parcel, defined as an arbitrary volume V_p [L^3] or mass $\rho_s V_p$ [*M*] of sediment that conceptually moves through the system as a coherent unit (where ρ_s [ML^{-3}] is the sediment density, the subscript *p* denotes a parcel, and the subscript *s* denotes sand). Spatially, parcels can be input anywhere along the length of any link. Temporally, these inputs can recur based on a specified interarrival time distribution.

2.3. Transport Dynamics

An individual parcel of sediment is conceptualized as moving through a link via a physically based time delay. Herein, we very briefly summarize the travel time derivation for bed material sand transport from *Czuba and Foufoula-Georgiou* [2014] that represents the travel time $t_{s,i,t}$ [*T*] of a sand parcel to move through link *i* at a particular time *t* in the absence of storage. An additional time delay due to storage is handled separately and is described in section 2.4. Through equations for uniform (normal) flow hydraulics and *Engelund and Hansen*'s [1967] sediment-transport formula for total bed material load, a volumetric transport rate of sand was estimated then decomposed into a bulk sand transport velocity and a cross-sectional area through which the majority of sand transport takes place. Travel time was then computed as the time it takes a sand parcel to move through a link of length ℓ_i at a bulk sand transport velocity. After combining these equations, the travel time reduces to

$$t_{s,i,t} = \frac{\theta_i g^{1/2} R_i^2 D_i}{0.05} \ell_i u_{w,i}^{-2} H_i^{-1/2} S_{i,t}^{-3/2}, \quad (1)$$

where θ_i is the fraction of the flow depth below which the "majority" of sand transport takes place (guidance on the selection of θ_i is provided in Appendix A), g [LT^{-2}] is the acceleration due to gravity, R_i is the submerged specific gravity of sediment in link *i*, D_i [L] is the sediment grain size in link *i*, $u_{w,i}$ [LT^{-1}] is the streamflow velocity in link *i*, and H_i [L] is the flow depth in link *i*. Equation (1) describes the travel time of a sand parcel through a link according to streamflow hydraulics specified by $u_{w,i}$ and H_i. While not explicitly stated, any variable can be specified as a function of spatial location for a given link *i*, vary with time *t*, or specified as a function of other variables. Only those variables that are allowed to vary with time in the model described herein are given the time index *t*. However, it is important to note that future model developments do not need to restrict temporal variability to only these variables. This means that equation (1) can be used to simulate the transport of sediment under explicit time-varying hydraulics.

2.4. Storage Dynamics

Both lake and in-channel storage were simulated in the present model. Lakes directly connected to the channel network acted as terminal bed material sinks as the residence time in lakes was assumed much longer than the transport timescale through the network. Thus, any sand parcels that entered a lake were

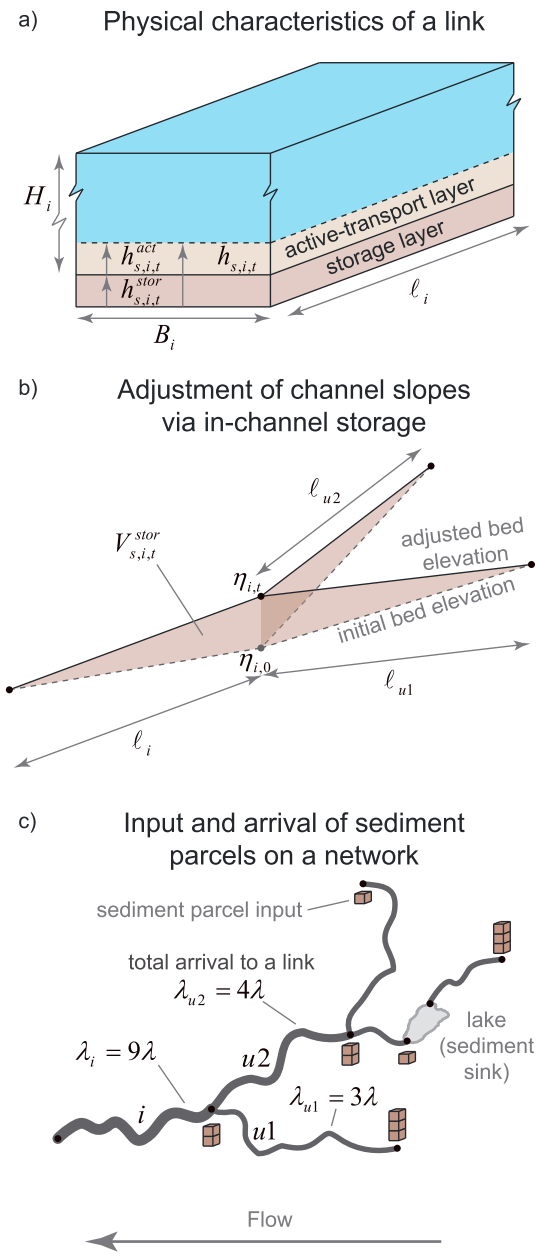

Figure 2. Schematic of model elements at various scales. (a) Link scale depicting the active-transport and storage layer. (b) Multilink storage scale depicting how a volume of sediment $V^{stor}_{s,i,t}$ at time t is placed in its immediate link and directly upstream links to adjust bed elevation and thus slopes. (c) River-network scale depicting how the arrival rate of sediment parcels changes progressing downstream. Each cube represents an individual parcel with rate λ input to the upstream end of a link. Lakes act as sediment sinks removing any sediment arriving from upstream from the system. See text for definition of symbols.

removed from the system. In-channel storage of parcels occurred whenever transport capacity was exceeded, the excess volume aggraded the bed, and thus adjusted the slope and thereby affected transport. These storage dynamics were briefly described by *Gran and Czuba* [2017], but here we refine this framework and provide more mathematical detail and greater insight into the inner workings of the model.

The volumetric transport rate of sand as computed from *Engelund and Hansen*'s [1967] sediment-transport formula defined transport capacity. We can think about this transport capacity in the context of the model as a volume or depth of sediment in a link. The volumetric transport rate of sand or transport capacity can be written as the volume of the active-transport layer at capacity χ_i [L^3] within a link divided by the travel time to move through that link $t_{s,i,t}$. The volume of the active-transport layer at capacity χ_i is given by

$$\chi_i = \ell_i(\theta_i H_i)B_i, \tag{2}$$

where B_i [L] is the channel width of link i. We can also convert this volume to a thickness of the active-transport layer at capacity $H_{s,i}$ [L] (Figure 2a) as

$$H_{s,i} = \frac{\theta_i H_i}{(1-\phi)}, \tag{3}$$

where ϕ is the porosity of the bed material sediment and the term $(1-\phi)$ effectively increases the volume occupied by the parcels on the bed due to pore space present in the subsurface deposit.

At every time t, we computed the total parcel volume in each link i as $V_{s,i,t}$ [L^3] and compared it to the volume of the active-transport layer at capacity χ_i. Any excess volume above capacity was considered as in-channel storage $V^{stor}_{s,i,t}$ [L^3] and was defined as follows:

$$V^{stor}_{s,i,t} = \begin{cases} V_{s,i,t} - \chi_i, & \text{if } V_{s,i,t} > \chi_i \\ 0, & \text{otherwise} \end{cases}. \tag{4}$$

The specific parcels that were placed into in-channel storage were those that first arrived into the link (following first in, last out) and whose cumulative volume was at least $V^{stor}_{s,i,t}$. These parcels were placed into in-channel storage by "pausing" their transport through the link (i.e., they did not move while in storage),

and they could only be released from in-channel storage (following last in, first out) when the supply of parcels transporting through the link decreased below capacity. This pausing of parcels above capacity resulted in an additional time delay to the travel time of a parcel through a link due to transport limitations associated with transient in-channel storage.

Any parcels placed into in-channel storage could subsequently be released, allowing the bed to return to its initial profile. However, new sediment inputs were not generated from the bed during supply-limited conditions. Instead, the bed at its initial profile was assumed to be bedrock floored or armored with a coarse lag deposit, and simulations then captured the dynamics of sand moving over a nonerodible substrate. This assumption was made because often the depth of alluvium is unknown and incision into the underlying alluvium (driven by a sediment-supply limitation) often results in a coarsening of the bed that reduces further incision [e.g., *Dietrich et al*., 1989; *Parker*, 2008]. Incorporating incision and the feedback dynamics controlling incision would require specifying particle-sorting dynamics and depth and grain-size distribution of the alluvium which is beyond the scope of this work.

Additionally, the volume of sediment placed into in-channel storage $V_{s,i,t}^{\mathrm{stor}}$ in link i was placed in such a way as to increase the channel slope of link i and simultaneously decrease the channel slope of the two directly upstream channel links (referred to with link indices $u1$ and $u2$; recall that links were defined between tributary junctions), consistent with principles of 1-D river morphodynamics [*Parker*, 2004]. The specific geometry for adjusting slopes in this way is shown in Figure 2b, where $V_{s,i,t}^{\mathrm{stor}}$ is placed in three wedges connected together at the upstream end of link i. Consistent with this geometry, bed elevation $\eta_{i,t}$ at the upstream end of link i was adjusted (for the case of two upstream tributary channel links) as

$$\eta_{i,t} = \eta_{i,0} + \frac{2V_{s,i,t}^{\mathrm{stor}}}{(B_i\ell_i + B_{u1}\ell_{u1} + B_{u2}\ell_{u2})(1-\phi)}, \tag{5}$$

where $\eta_{i,0}$ [L] is the initial elevation at the upstream end of link i at time $t = 0$. We assumed sufficiently low slopes such that the three-dimensional distance between ends of a link ℓ_i was approximately equal to the two-dimensional horizontal distance between the ends of a link (Figure 2b). For the case of only one upstream channel link $u1$, equation (5) would only contain two $B\ell$ terms, instead of three, with indices i and $u1$, and in the absence of any upstream channel links, equation (5) would only contain the $B_i\ell_i$ term. Sediment parcels in storage in link i always resided in link i (for tracking their movement through the network), but this conceptual placement of that storage volume ensured smooth slopes consistent with changes in bed elevation.

Once $\eta_{i,t}$ was computed for all links at time t, then the channel slope $S_{i,t}$ was recomputed for all links as

$$S_{i,t} = \frac{\eta_{i,t} - \eta_{d,t}}{\ell_i}, \tag{6}$$

where $\eta_{d,t}$ denotes the elevation at the downstream end of link i, as the index d denotes the index of the link directly downstream of link i. In this formulation, the elevation of the basin outlet was fixed at its initial value through time. Recall that the volumetric transport rate of sand or transport capacity can be written as the volume of the active-transport layer at capacity χ_i within a link divided by the travel time to move through that link $t_{s,i,t}$. Changes in slope due to in-channel storage affected transport capacity by altering travel time $t_{s,i,t}$ via equation (1); however, the volume of the active-transport layer at capacity χ_i remained unchanged because we do not specifically account for the feedback between channel slope and θ_i (see equation (2) and Appendix A). This simplification has a negligible effect on the results and does not change our conclusions. The effects of storage were not only local to an individual link but also propagated to channel links directly upstream.

2.5. Analytical Insights

With the model described herein we simulated the bed sediment thickness $h_{s,i,t}$ [L] that accumulated upon the initial bed during a given simulation period, computed as

$$h_{s,i,t} = \frac{V_{s,i,t}}{B_i\ell_i(1-\phi)}. \tag{7}$$

This bed sediment thickness should not be mistaken for the total depth of alluvium that may occur in a given reach (i.e., the deeper reservoir of sediment below the initial bed that this model does not track nor incise

into). In this section, we describe how the mean and pdf of bed sediment thickness in a given link can be computed analytically under further assumptions (that frame the problem as a Poisson arrival process) without the need for numerical simulations. These analytical results are useful because they not only establish the mathematical relation between bed sediment thickness, sediment supply, sediment transport, and channel characteristics but also provide a way to obtain some results more quickly and simply through analytical computation rather than through numerical simulations.

Analytically, we separately compute the thickness of an active-transport layer $h_{s,i,t}^{\text{act}}$ [L] and a storage layer $h_{s,i,t}^{\text{stor}}$ [L] which together equate to the bed sediment thickness $h_{s,i,t}$ (see Figure 2a) as

$$h_{s,i,t} = h_{s,i,t}^{\text{act}} + h_{s,i,t}^{\text{stor}}, \tag{8}$$

and we represent their time averages with an overbar (i.e., $\overline{h}_{s,i}^{\text{act}}$, $\overline{h}_{s,i}^{\text{stor}}$, and $\overline{h}_{s,i}$). All thicknesses associated with bed material sediment herein included the $(1-\phi)$ term that accounts for sediment porosity of the resulting deposit. The time-averaged thickness of the active-transport layer $\overline{h}_{s,i}^{\text{act}}$ is

$$\overline{h}_{s,i}^{\text{act}} = \begin{cases} H_{s,i}, & \text{if } \overline{h}_{s,i}^{\text{stor}} > 0 \\ \overline{h}_{s,i} \leq H_{s,i}, & \text{if } \overline{h}_{s,i}^{\text{stor}} = 0 \end{cases}. \tag{9}$$

Thus, on average, during transport-limited conditions (i.e., when supply rate is greater than transport rate and "activates" in-channel storage), the simulated transport rate is at transport capacity ($\chi_i/t_{s,i,t}$). During supply-limited conditions (i.e., when transport rate is greater than supply rate and does not activate in-channel storage), the simulated transport rate is less than transport capacity as $V_{s,i,t}/t_{s,i,t}$, where $V_{s,i,t} < \chi_i$.

We conceptualize the spatially variable sediment supply to the river network as sediment parcels arriving at each link of the network according to a Poisson process. A Poisson (arrival) process is a stochastic process with convenient mathematical properties often used to model independent events such as storm arrival [e.g., *Rodriguez-Iturbe and Eagleson*, 1987], for example. In geomorphology, a Poisson process has been used to model the occurrence of tectonic movements in a simulation model of alluvial stratigraphy [*Bridge and Leeder*, 1979], to derive a theoretical Strahler stream length distribution [*Yang and Lee*, 2001], to model episodic surface denudation by the spalling off of slabs of rock at discrete times [*Muzikar*, 2008], and to model the effect of rainfall variability on landscape evolution [*Tucker and Bras*, 2000], among others. One important property of the Poisson process is that each arrival is stochastically independent from all other arrivals, meaning that this is a completely random process. If we denote by λ [T^{-1}] the arrival rate of events, then it can be shown that the time between events has an exponential distribution with mean λ^{-1} and that the sum of events arriving during a period of time t has a Poisson distribution with mean λt [e.g., *Durrett*, 2012]. We take these properties into consideration in the derivations that follow.

To cast the watershed sediment supply problem as a Poisson arrival process on the links of the river network, we must first decompose an arbitrary magnitude input from a sediment-generating feature into a number of parcels each with volume V_p that are each then independently delivered to the network according to a Poisson process with rate λ (and thus mean and standard deviation of interarrival times equal to λ^{-1}). Breaking the inputs in this way means that the arrival of parcels to link i from all upstream tributary links supplying sediment and those generated internally will also follow a Poisson process with rate λ_i [T^{-1}] as

$$\lambda_i = n_i \lambda, \tag{10}$$

where n_i is the total number of inputs of volume V_p upstream of link i but downstream of any lakes directly connected to the network (Figure 2c). Note that n_i is not simply the number of upstream links but also incorporates the magnitude of the input to each upstream link in increments of V_p.

For supply-limited conditions in link i and upstream, $h_{s,i,t}^{\text{act}} = h_{s,i,t}$, and thus, the pdf of $h_{s,i,t}^{\text{act}}$, $f\left(h_{s,i,t}^{\text{act}}\right)$, is equal to the pdf of $h_{s,i,t}$, $f(h_{s,i,t})$. At quasi steady state, once a parcel arrives to a link, it remains in that link, on average, for a duration of $\overline{t}_{s,i}$ [T], which is the time-averaged travel time for a sand parcel to move through a link. During supply-limited conditions, slope never changes, and thus, $\overline{t}_{s,i}$ is equivalent to the initial travel time $t_{s,i,0}$ at time

$t = 0$. According to the Poisson arrival process, the number of parcels N_i within link i for duration $\bar{t}_{s,i}$ is given by the Poisson distribution $f\left(k;\lambda_i\bar{t}_{s,i}\right)$ as

$$f\left(k;\lambda_i\bar{t}_{s,i}\right) = \Pr\left[N_i\left(t+\bar{t}_{s,i}\right) - N_i(t) = k\right] = \frac{\left(\lambda_i\bar{t}_{s,i}\right)^k e^{-\left(\lambda_i\bar{t}_{s,i}\right)}}{k!}, \tag{11}$$

where $k = 0, 1, 2, \ldots$ and with both mean and variance equal to $\lambda_i\bar{t}_{s,i}$ [*Durrett*, 2012]. The pdf of the thickness of the active-transport layer $f\left(h^{\text{act}}_{s,i,t}\right)$ is then just a scaled Poisson distribution as

$$f\left(h^{\text{act}}_{s,i,t}\right) = \frac{V_p f\left(k;\lambda_i\bar{t}_{s,i}\right)}{B_i\ell_i(1-\phi)}, \tag{12}$$

which for supply-limited conditions is equivalent to $f(h_{s,i,t})$. On average, the volume of sediment in link i is given by $V_p\lambda_i\bar{t}_{s,i}$ and the quantity $V_p\lambda_i$ represents the volumetric supply rate of sediment to link i. Therefore, the time-averaged thickness of the active-transport layer $\overline{h}^{\text{act}}_{s,i}$ is given by

$$\overline{h}^{\text{act}}_{s,i} = \frac{V_p\lambda_i\bar{t}_{s,i}}{B_i\ell_i(1-\phi)} = \frac{V_p n_i\lambda\bar{t}_{s,i}}{B_i\ell_i(1-\phi)}, \tag{13}$$

which for supply-limited conditions is equivalent to $\overline{h}_{s,i}$. These analytical results refer to only the thickness of the active-transport layer because we must assume that $V_p\lambda_i$ is the average volumetric supply rate both arriving and departing at a given time, which is not the case with storage.

For transport-limited conditions, the storage process disrupts the transport of parcels in a way that alters the Poisson arrival process such that the analytical results for $f(h_{s,i,t})$ (via equation (12)) do not hold. However, we can still compute $\overline{h}_{s,i}$ as the sum of $\overline{h}^{\text{act}}_{s,i}$ (equation (13)) and $\overline{h}^{\text{stor}}_{s,i}$. An iterative procedure is required for calculating $\overline{h}^{\text{stor}}_{s,i}$ which is presented in Appendix B. Then, we can provide an estimate of $f(h_{s,i,t})$, referred to as $\hat{f}\left(h_{s,i,t}\right)$ computed as $f\left(h^{\text{act}}_{s,i,t} + \overline{h}^{\text{stor}}_{s,i}\right)$, which preserves the mean of $f(h_{s,i,t})$ but with a variance always less than that of $f(h_{s,i,t})$. We compare this estimated pdf $\hat{f}\left(h_{s,i,t}\right)$ to $f(h_{s,i,t})$ computed from numerical simulations to isolate the influence of river-network structure on bed material sediment dynamics. As discussed in the application below, this comparison leads to insights about how in-channel storage in links of the network affects downstream reaches.

3. Application to the Greater Blue Earth River Basin

The network-based modeling framework for bed material sediment was applied to the Greater Blue Earth River Basin. The landscape setting is first described in section 3.1. Details on the application of the framework to this basin include a description of the river network (section 3.2), the specific spatial distribution and magnitude of sediment inputs derived from a sediment budget (section 3.3), and the transport and storage dynamics (section 3.4). This section ends with an overview of model simulations (section 3.5).

3.1. Landscape Setting

The Greater Blue Earth River Basin includes the Le Sueur River Basin and drains 9200 km^2 of southern Minnesota and northern Iowa to the Minnesota River (Figure 3). The basin was glaciated multiple times throughout the Pleistocene, the effects of which exert considerable control on geomorphic dynamics today [see *Ojakangas and Matsch*, 1982; *Gran et al.*, 2013]. During glacial retreat, a proglacial lake, known as glacial Lake Minnesota, formed across a large portion of the Greater Blue Earth River Basin depositing fine surficial sediments [*Ojakangas and Matsch*, 1982]. When glacial Lake Agassiz drained through its southern outlet 13,400 cal years B.P. (calendar years before present) to carve the present-day Minnesota River valley [*Clayton and Moran*, 1982], the base-level of the Greater Blue Earth River was lowered by roughly 70 m. This lowering created a knickpoint, or sharp break in channel slope, at the outlet of the river that has since migrated 40–60 km upstream (Figure 3), leaving a rapidly incising knickzone in its wake [*Gran et al.*, 2009, 2013; *Belmont*, 2011; *Belmont et al.*, 2011]. Today, channel slopes in major rivers of the basin upstream of the knickzone are on the order of 1×10^{-4} to 1×10^{-3} and within the knickzone increase to roughly over 1×10^{-3} [see *Czuba and Foufoula-Georgiou*, 2015, Figure 3]. Incision in this basin is localized to the knickzone, where the bed is incising into till (with roughly 3% gravel) coarsening the bed as incision progresses.

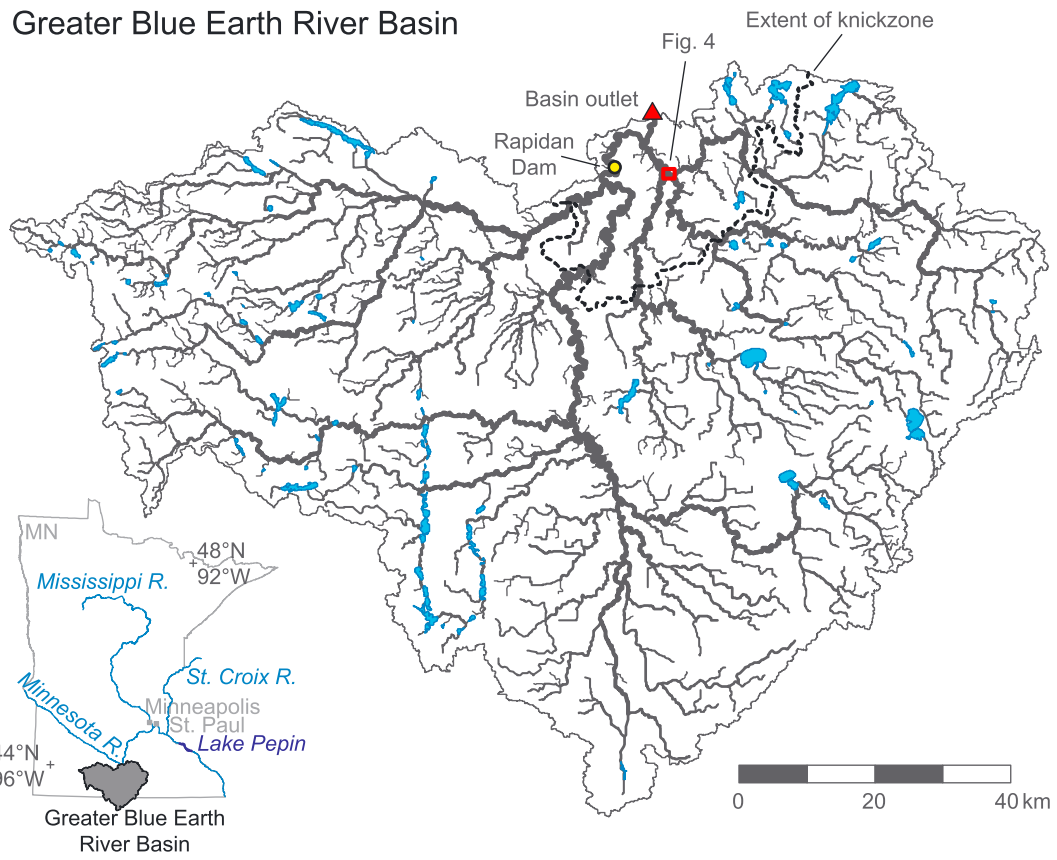

Figure 3. Study area map of the Greater Blue Earth River Basin. A detailed basin map shows the channel network (gray; thicker lines correspond to reaches with larger upstream drainage areas), lakes incorporated into the model (light blue), and the approximate extent of the knickzone (black dashed line). Location and extent of Figure 4 is shown by a small red box. Inset shows a location map of the Greater Blue Earth River Basin relative to the State of Minnesota.

Upstream of the knickzone, streams meander through low-gradient uplands, and straightened, agricultural drainage ditches are common first-order channels.

Like many Midwestern U.S. landscapes, agriculture is the dominant (85%) land use in the basin [*Jin et al.*, 2013]. Many of the wetlands that once dotted the landscape have been drained beginning in the late 1800s by surface ditches and subsurface drain tiles. The extensive subsurface drainage system has reduced surface erosion from upland fields, but at the expense of amplifying streamflows, accelerating near-channel erosion of downstream banks and bluffs and initiating stream morphologic changes such as channel widening [*Belmont et al.*, 2011; *Lenhart et al.*, 2013; *Schottler et al.*, 2014; *Foufoula-Georgiou et al.*, 2015]. While the Greater Blue Earth River Basin has historically exported a large amount of sediment compared to surrounding basins, the amount of sediment deposited downstream in Lake Pepin has increased by about an order of magnitude in just over a century [*Kelley and Nater*, 2000]. This is in part due to the presence of large bluffs adjacent to the river that make sediment generation in the basin highly sensitive to changes in streamflow. However, turbidity is just one of many water-quality impairments in the basin [*Minnesota Pollution Control Agency*, 2014] contributing to a decline in macroinvertebrates, sensitive fish species, and native mussels [*Kirsch et al.*, 1985; *Musser et al.*, 2009; *Carlisle et al.*, 2013; *Hansen et al.*, 2016].

3.2. Network of River Channels and Lakes

The underlying structure of the model is the river network, obtained from the National Hydrography Dataset Plus Version 2 (NHDPlusV2) [*McKay et al.*, 2012; *Horizon Systems*, 2014]. As part of the NHDPlusV2 river network, each link has been associated with relevant topologic and physical attributes as described previously in section 2.1. Lake polygons were obtained from the waterbody feature of the NHDPlusV2 data set [*McKay et al.*, 2012; *Horizon Systems*, 2014]. Only lake polygons that intersect the river network and have surface

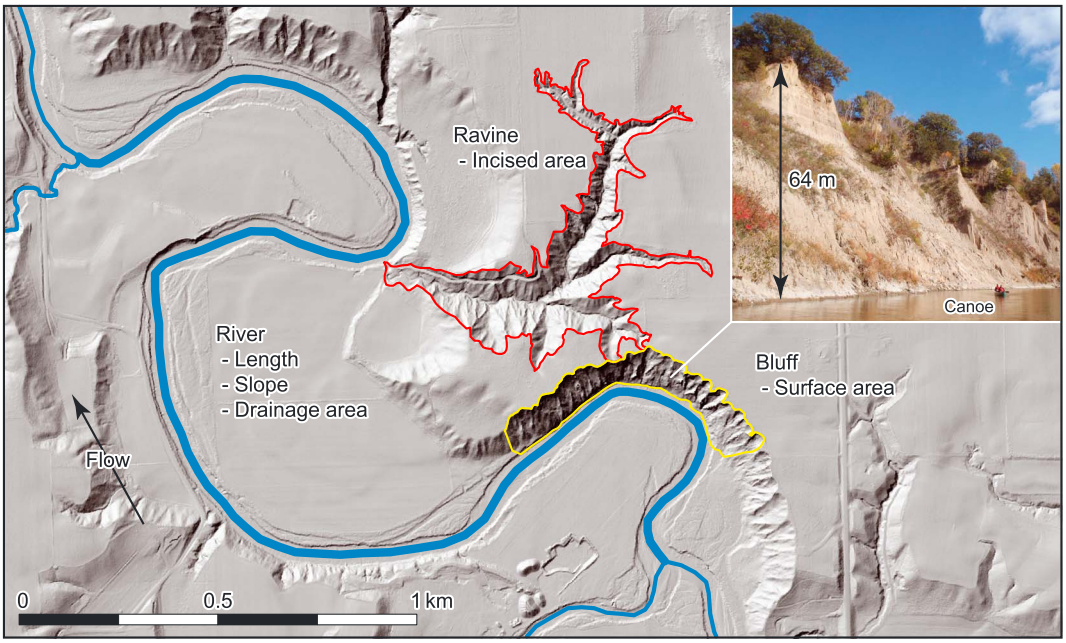

Figure 4. Lidar hillshade highlighting major features (river, bluff, and ravine, each with relevant attributes) incorporated into the model. Inset image shows a 64 m bluff; note the canoe for scale. Location and extent is shown in Figure 3 by a small red box.

area >0.04 km^2 were incorporated into the network as individual lake links (Figure 3). The NHDPlusV2 network was preprocessed by (1) clipping to the extent of the Greater Blue Earth River Basin; (2) removing isolated and secondary channels; (3) establishing a new set of links with index *i*, with a link defined between tributary junctions, as the intersection of a lake polygon with the network, or between a lake polygon and a junction; and (4) mapping or computing attributes for each link from the original NHDPlusV2 network. The final network was composed of 1253 channel links and 107 lake links for a total of 1360 links.

3.3. Inputs From a Sediment Budget

Fine sediment (silt and clay) budgets of the Greater Blue Earth River Basin [*Bevis*, 2015] and the Le Sueur River Basin [*Gran et al.,* 2011; *Belmont et al.,* 2011] constrain the location, magnitude, and frequency of sediment inputs from bluffs, streambanks, ravines, and uplands (mainly low-gradient agricultural fields). Bed material throughout the Greater Blue Earth River Basin is primarily sand [*U.S. Geological Survey*, 2014], and only sand is represented in the model. Grain-size distributions measured for till and surficial soils were used to convert the fine-sediment inputs quantified in the sediment budget to sand inputs. Although gravel in the bed material can play a role in setting bed roughness and in slowing channel incision [*Gran et al*., 2013], gravel is only a small portion of the bed load and is not tracked here. Only inputs from bluffs, ravines, and uplands (Figures 4 and 5) were incorporated into the present model. Details on how we quantified sand inputs from each of these sources are provided in Appendix C. The knickzone is incising at a rate of 2.6 mm yr^{-1} [*Gran et al*., 2013] but contributes less than 2% of sediment to the fine-sediment budget on the Le Sueur River [*Gran et al*., 2011; *Belmont et al*., 2011]. Net sediment contributions (+7 Mg yr^{-1}) from streambank erosion (+43 Mg yr^{-1}, from migration and widening) and floodplain deposition ($-$36 Mg yr^{-1}) are also a small component (3% of sediment) to the Le Sueur fine-sediment budget [*Gran et al*., 2011; *Belmont et al*., 2011]. Representation of these exchange dynamics requires further developments of the model [e.g., *Lauer and Willenbring*, 2010; *Viparelli et al*., 2013; *Lauer et al*., 2016] and is beyond the scope of the present study.

3.4. Transport and Storage Dynamics

Herein, downstream hydraulic geometry relations were used to parameterize $u_{w,i}$ and H_i (where frictional losses are implicit) at bankfull flow (specifically at the 2 year recurrence interval peak flow) as a function of upstream drainage area A_i. Under this parameterization of streamflow hydraulics, the travel time in equation (1) for a constant bankfull flow must be converted to real time through an intermittency factor $I_{f,s}$

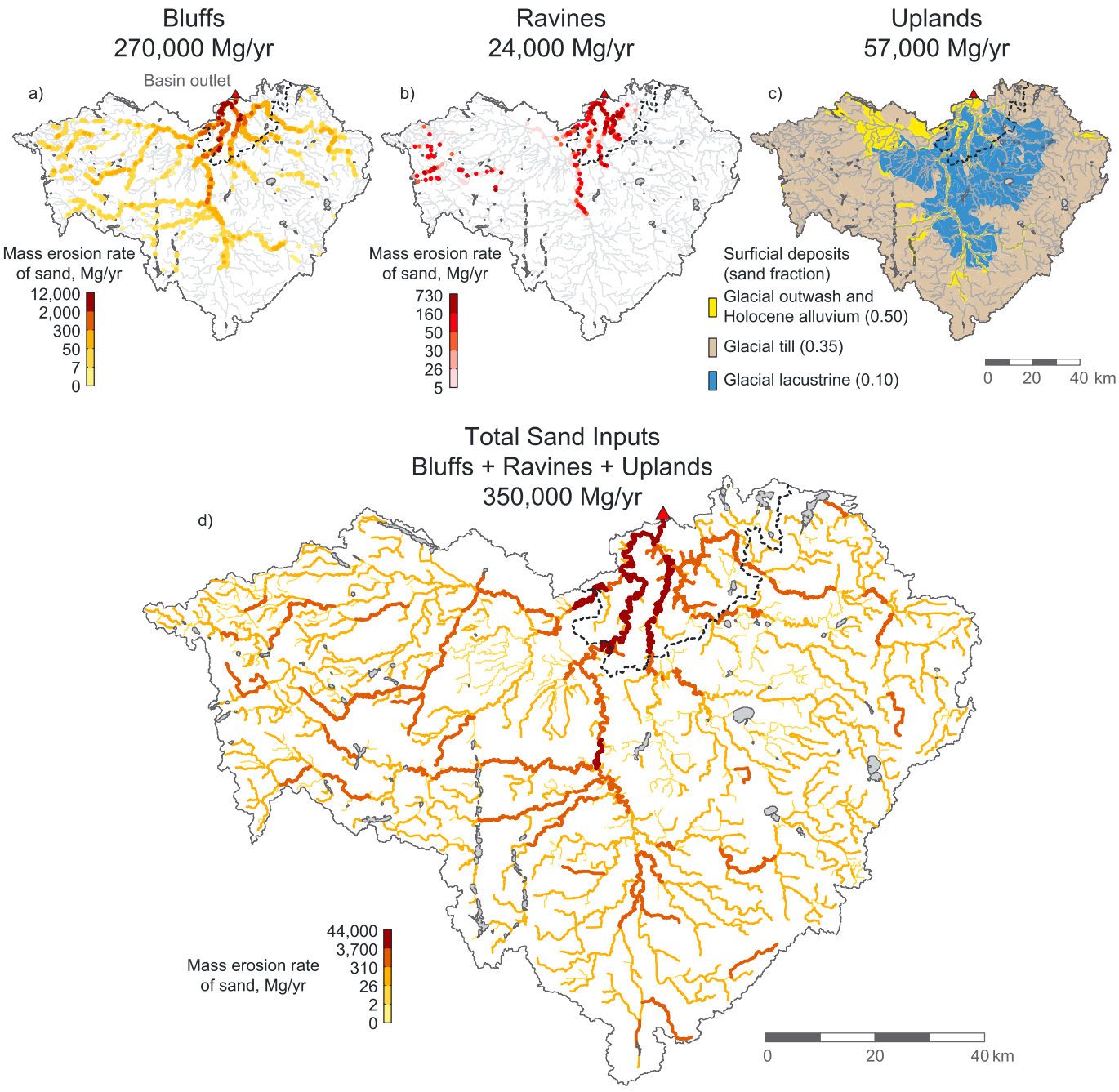

Figure 5. Spatially variable and temporally Poisson process (independent arrival) of sediment supply. (a) Bluff locations colored by mass erosion rate of sand from each bluff. (b) Ravine locations colored by mass erosion rate of sand from each ravine. (c) Uplands with surficial deposits and sand fraction. (d) Total sand input delivered to each link of the network from bluffs, ravines, and uplands. The approximate extent of the knickzone is shown as a dashed line.

[*Paola et al.*, 1992; *Parker*, 2004]. The intermittency factor denotes the fraction of time per year that continuous bankfull flow would yield the mean annual sand load (see *Czuba and Foufoula-Georgiou* [2014] for details). The result averages over the intermittent short periods with intense transport and long periods with low transport to represent a continuous long-term (more than tens of years) probabilistic-average transport of sediment. Therefore, equation (1) becomes

$$t_{s,i,t} = \frac{\theta_i\, g^{1/2} R_i^2 D_i}{0.05 \alpha_{u_w A}^2 \alpha_{HA}^{1/2} I_{f,s}} \ell_i A_i^{-\left(2\beta_{u_w A} + \beta_{HA}/2\right)} S_{i,t}^{-3/2}, \tag{14}$$

where α_{u_wA} and α_{HA} are empirically derived coefficients and β_{u_wA} and β_{HA} are empirically derived exponents of the downstream hydraulic geometry scaling relations for flow velocity and depth. We do not account for nonstationary discharge in this basin [*Novotny and Stefan*, 2007; *Dadaser-Celik and Stefan*, 2009; *Foufoula-Georgiou et al*., 2015], but this could be handled in equation (14) by specifying a time-varying intermittency factor or by allowing the coefficients and exponents of the hydraulic geometry relations to vary in time. Changes in the flow regime will also affect channel properties (such as width) [*Schottler et al*., 2014] and sediment generation [*Belmont et al*., 2011]; in the present formulation the relevant variables (e.g., channel width, sediment input rate, and hydraulic geometry relation) can become time varying. However, the incorporation of autogenic sediment generation and feedbacks between flow and channel response (partitioning between changes in roughness/grain size, width, and slope) are presently limited by our understanding of these processes.

The travel time $t_{s,i,t}$ of a sand parcel to move through a link was reduced to a function of only link properties by assigning the following parameters: $g = 9.81$ m s^{-2}, $\theta_i = 0.1$ ($\forall i$, i.e., for all i; assuming the majority of sand transport occurs in the lower 10% of the flow depth, see also Appendix A), $R_i = 1.65$ ($\forall i$), $D_i = 4 \times 10^{-4}$ m ($\forall i$; D50 size of sand from riverbed material) [*U.S. Geological Survey*, 2014], $\alpha_{u_wA} = 0.20$, $\beta_{u_wA} = 0.07$, $\alpha_{HA} = 2.9 \times 10^{-3}$, and $\beta_{HA} = 0.29$ (computed at the 2 year recurrence interval peak flow and using streamflow and channel cross-sectional properties of 23 stations; here A_i is specified in m^2, H_i in m, and $u_{w,i}$ in m s^{-1}; see Appendix A of *Czuba and Foufoula-Georgiou* [2014] for details), and $I_f = 0.175$ (computed from a flow-duration curve; see Appendix B of *Czuba and Foufoula-Georgiou* [2014] for details). Substituting these parameters into equation (14) reduces the travel time $t_{s,i,t}$ to

$$t_{s,i,t} = 18\ell_i A_i^{-0.285} S_{i,t}^{-3/2}, \tag{15}$$

where ℓ_i is specified in meters and thus $t_{s,i,t}$ is given in seconds. The intermittency factor introduced in equation (14) and embedded in the coefficient of equation (15) means that all times reported from here on refer to real time or calendar years.

For storage in lakes, upstream drainage area and lake volume were used to compute, through an empirical relation, trapping efficiencies for fine sediment [*Brown*, 1943; *Bevis*, 2015]. The average fine sediment trapping efficiency for the lakes included in the model was 91% [*Bevis*, 2015]. Thus, the sand trapping efficiency for these lakes was assumed at 100%, and any sand parcels that entered a lake were removed from the system.

3.5. Overview of Simulation

The model simulation began at time $t = 0$ and ran for 600 cal years. Sediment parcels were introduced independently to each link according to the spatial pattern and magnitude as specified by the sediment budget (Figure 5d) with parcel volume $V_p = 10$ m^3 for all parcels and following an exponential interarrival time distribution with $\lambda = 1$ yr^{-1} (to align with annualized sediment budget input volumes). For example, a long-term input rate of 63 m^3 yr^{-1} would be broken into six parcels each as independent inputs recurring through time with interarrival times randomly selected from an exponential distribution with a mean recurrence of 1 cal year (as six parcels of volume $V_p = 10$ m^3 with $\lambda = 1$ yr^{-1} equates to 60 m^3 yr^{-1} and we ignore the small remainder of 3 m^3 yr^{-1}). The frequency of an input could very well differ between different sediment sources, although the magnitude and frequency of an input should be selected to be consistent with the generation rate (i.e., we could have input a single parcel with magnitude of 63 m^3 and average interarrival time of 1 year to be consistent with a rate of 63 m^3 yr^{-1}). But we chose the magnitude/frequency of inputs to be consistent with the analytical results, which required constant parcel volume, independent inputs, and exponential interarrival time distribution. Accurately specifying inputs requires understanding not only the rate of sediment generation but also the specific magnitude/frequency characteristics of sediment generation for each source. The parcel volume was selected to balance a volume as small as possible with a computationally manageable number of parcels; over 600 years nearly eight million parcels were tracked through the system.

Sediment dynamics in the river network were tracked at a temporal resolution of 20 time steps per calendar year, i.e., the modeling time step was set at 18.25 days. Parcels were tracked as they moved through each link with transport-related properties resulting in a time delay given by equation (15). For reference, the average travel time through a link was computed and was found to be just over 1 year. If at any time there were more parcels in a given link than could be moved at capacity (equation (4)), then a subset of parcels would enter in-

channel storage, and the slope of that link and directly upstream links would be adjusted at the next time step. It took less than 200 years for an input at the farthest upstream location to exit the basin at the outlet, for the bed sediment to build up in channel links, and for the bed adjustment to achieve quasi-steady state. Thus, all statistics computed from the simulation model only include results between time 200 and 600 years.

Mass of sediment was interchanged into volume of sediment using a sediment density $\rho_s = 2.65$ Mg m^{-3}, and bed sediment thickness was computed using a bed sediment porosity $\phi = 0.4$ [*Wu and Wang*, 2006]. A minimum channel slope of 1×10^{-5} was imposed in the model to avoid artificially low slopes from DEM processing of backwater areas. Also, the effect of Rapidan Dam, located on the Blue Earth River near the basin outlet (Figure 3), was removed because the reservoir, which has been dredged multiple times, is mostly full of sediment, some sand likely passes the dam, and we are not trying to capture the system exactly as it is nor quantitatively predict sediment leaving the basin. The dam was removed by selecting a channel slope for the links upstream and downstream of the dam that linearly connected the bed elevations between unaffected upstream and downstream points. Bed elevations were then recomputed from the basin outlet in order to establish consistency between $\eta_{i,0}$ and $S_{i,0}$. Due to the presence of some very short links in the network (<300 m) that arose between closely spaced tributaries, some links had a very small volume of the active-transport layer at capacity resulting in an artificial bottleneck in the network. To circumvent this issue, a minimum volume of the active-transport layer at capacity for these short links was set as the maximum of (i) the volume of the active-transport layer at capacity of the link computed via equation (2), (ii) the volume of the active-transport layer at capacity of directly upstream links, or (iii) 100 m^3, which ensured at least 10 parcels could move through a link at a given time.

We set up the model in three different ways to achieve different goals: (1) to simulate sediment input, transport, and storage dynamics on a river network as described by the model formulation herein (referred to as the "network, in-channel storage" model); (2) to directly confirm the analytical results by turning the in-channel storage mechanism off (referred to as the "network, no in-channel storage" model); and (3) to help isolate the role of network hierarchical structuring (referred to as the "single link, in-channel storage" model). In the "single link, in-channel storage" model, we maintained the full dynamics described for the network, in-channel storage model but isolated the sediment supply to each link and replaced it with one that was guaranteed to follow a Poisson arrival process with the same supply rate. This allowed us to isolate differences in the time series of bed sediment thickness between in-channel storage processes occurring locally and those occurring farther upstream whose effects have propagated downstream. The storage reservoir for adjusting the slope of a link in the single link, in-channel storage model still accounted for the width and length of directly upstream links (as in equation (5) and Figure 2b); however, each link was disconnected from its directly downstream link and from any slope adjustments resulting from downstream in-channel storage.

4. Analytical and Simulated Bed Material Sediment Dynamics

To first verify that the model was working as expected, the network, no in-channel storage model was run. Interarrival times of sediment parcels to each link in the network followed an exponential distribution with parameter λ_i as in equation (10). Additionally, the number of parcels within each link (or bed sediment thickness) had a Poisson distribution with parameter $\lambda_i \bar{t}_{s,i}$ as in equation (11) (these results are not shown).

Before running the model, we identified where in the network transport capacity was exceeded by computing the initial ratio of sand supply relative to transport capacity or the relative capacity $RC_i^{iter=1}$, where iter denotes the current iteration (Figure 6a; see Appendix B for details). We determined, following the iterative procedure outlined in Appendix B, to what elevation, and thus slope, the bed must adjust to in order to pass the sediment supply. Doing so required adjusting slopes until $RC_i^{final} \leq 1$ (without performing model simulations); for this basin four iterations were necessary. The links where channel slopes increased are identified in Figure 6b by the equivalent amount of sediment that must build up on the bed to achieve that slope, or the thickness of the storage layer $\overline{h}_{s,i}^{stor}$. Although not indicated, the links directly upstream of the links identified in Figure 6b had lower slopes due to the adjustment in bed elevation. The final RC_i^{final} values after bed elevations had been adjusted throughout the network are shown in Figure 6c. Note that any $RC_i^{iter=1} > 1$ in Figure 6a are the locations where sediment was stored as $\overline{h}_{s,i}^{stor}$ in Figure 6b and whose RC_i^{final} values become equal to one in Figure 6c.

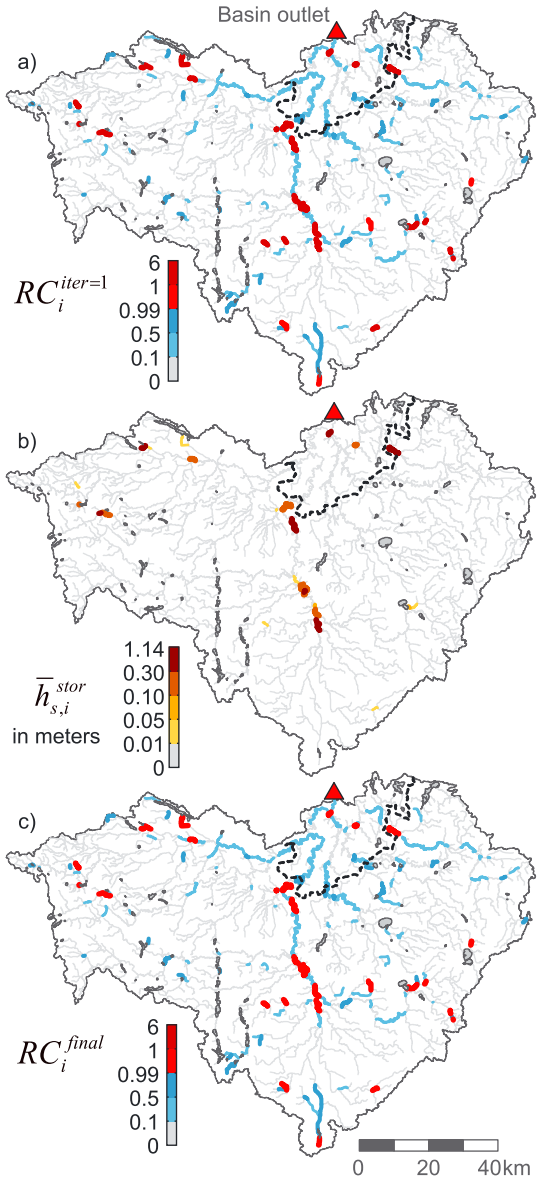

Figure 6. Identifying where and how much the bed must adjust so sand transport balances supply. (a) Initial ratio of sand supply relative to transport capacity $RC_i^{iter=1}$ (RC—relative capacity); a value of one indicates capacity balances supply. (b) Equivalent thickness of sediment that must build up on the bed to achieve a slope required to transport the sand supply $\overline{h}_{s,i}^{stor}$; note that these locations are where the values in Figure 6a are greater than one. (c) Final ratio of sand supply relative to transport capacity RC_i^{final} after the bed has adjusted to pass the supply; note any values in Figure 6a that were greater than one become equal to one. The approximate extent of the knickzone is shown as a dashed line. See text for definition of symbols.

Results of bed sediment thickness from the network, in-channel storage model are shown in Figure 7. The mean bed sediment thickness $\overline{h}_{s,i}$ throughout the river network shows that reaches along the main stem rivers just upstream of the knickzone accumulate bed material sediment (Figure 7a, shown as analytical mean bed sediment thickness and confirmed by direct simulation in Figure 7b). Under supply-limited conditions, the pdf $f(h_{s,i,t})$ of simulated bed sediment thickness (blue solid bars) was nearly the same as the estimated pdf $\hat{f}(h_{s,i,t})$ (black dashed line; Figure 7e). However, under transport-limited conditions, the pdf of bed sediment thickness $f(h_{s,i,t})$ was very different from $\hat{f}(h_{s,i,t})$, with much heavier tails than were predicted by a Poisson distribution (Figures 7c, 7d, and 7f). An asymmetric pdf with a very long tail was found for the link highlighted in Figure 7f, which looks much different in character than the others shown, and a trimodal pdf was found for the link highlighted in Figure 7d, related to its close proximity to a few major upstream tributaries. Also, the time series of bed sediment thickness exhibited periodicities with different timescales that were much greater than that of the sediment supply forcing timescale of 1 year. For much of the remainder of this paper, we focus on describing the characteristics of the system that give rise to the emergent behavior of bed sediment thickness, specifically heavy tails in the pdf and periodicity in the time series, to gain insight into bed material sediment dynamics on river networks.

In order to separate the temporal variability of bed sediment thickness that is internally generated by a single link from the variability that is propagated, amplified, or dampened from upstream links in the network, simulation results from the single link, in-channel storage model were compared to those from the network, in-channel storage model. Recall that for a Poisson distribution with parameter $\lambda_i \overline{t}_{s,i}$, the mean and variance are both equal to $\lambda_i \overline{t}_{s,i}$. Thus, the coefficient of variation COV_i defined as the ratio of the standard deviation to the mean is given by

$$COV_i = \frac{\sqrt{\lambda_i \overline{t}_{s,i}}}{\lambda_i \overline{t}_{s,i}} = \left(\lambda_i \overline{t}_{s,i}\right)^{-1/2}. \quad (16)$$

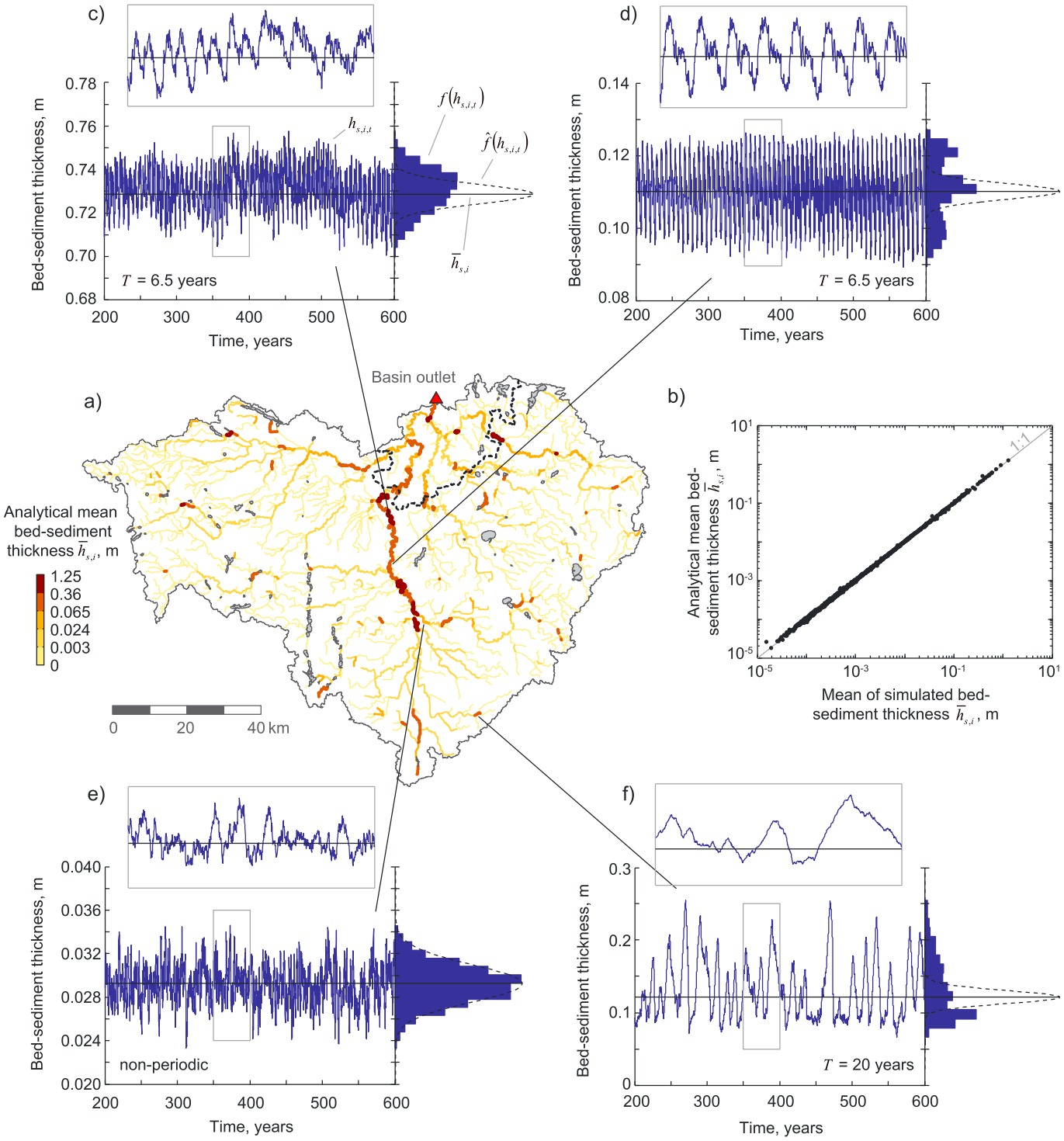

Figure 7. Simulated and analytical bed sediment thickness with in-channel storage. (a) Analytical mean bed sediment thickness $\overline{h}_{s,i}$ (see equation (13)). The color breaks are at the 0.99, 0.95, 0.90, and 0.75 quantiles. The approximate extent of the knickzone is shown as a dashed line. (b) Simulated mean bed sediment thickness averaged from 200 to 600 years versus the analytical mean bed sediment thickness $\overline{h}_{s,i}$. (c–f) Simulated bed sediment thickness $h_{s,i,t}$ with probability distribution function (pdf) $f(h_{s,i,t})$ shown at the right (blue). The solid horizontal line denotes the analytical mean bed sediment thickness $\overline{h}_{s,i}$. The estimated pdf $\hat{f}(h_{s,i,t})$ that assumes the in-channel storage process preserves the structure of a Poisson arrival process is shown at the right (black dashed; see equation (12) and discussion at the end of section 2.5). Inset box zooms in on the simulated bed sediment thickness time series between 350 and 400 years. The dominant period T of the bed sediment thickness time series (i.e., the time period corresponding to the peak of the Fourier transform) is also indicated. See text for definition of symbols.

For supply-limited conditions, the COV_i of simulated bed sediment thickness follows equation (16). For many links, the COV_i of simulated bed sediment thickness computed from the network, in-channel storage model (magenta, each point represents one link; Figure 8a) and from the single link, in-channel storage model (black; Figure 8a) follows equation (16). However, a number of links (points in Figure 8) deviate from this line indicating that the temporal variability of their bed sediment thickness was much larger than estimated from a Poisson distribution due to the in-channel storage process. We have quantified this deviation $dCOV_i$ by the relative difference between the COV_i of simulated bed sediment thickness and the COV_i predicted by equation (16) (Figure 8b, also indicated by arrow in Figure 8a) as

$$dCOV_i = \frac{\frac{\sigma_{h_{s,i}}}{\overline{h}_{s,i}^{act}} - \left(\lambda_i \overline{t}_{s,i}\right)^{-1/2}}{\left(\lambda_i \overline{t}_{s,i}\right)^{-1/2}}, \tag{17}$$

where $\sigma_{h_{s,i}}$ [L] is the standard deviation of the simulated bed sediment thickness $h_{s,i,t}$. The mean of the simulated thickness of the active-transport layer $\overline{h}_{s,i}^{act} = \overline{h}_{s,i} - \overline{h}_{s,i}^{stor}$ is used rather than $\overline{h}_{s,i}$ because the variability of $\sigma_{h_{s,i}}$ is related to $\overline{h}_{s,i}^{act}$ for this Poisson distribution.

The deviation $dCOV_i$ from only the single link, in-channel storage model simulations (black points) was then plotted against other variables (Figures 8c and 8d) to identify the internal link factors that led to the emergence of such large temporal variability in bed sediment thickness. Perhaps unsurprisingly, we see that the deviation $dCOV_i$ arises in links at capacity (Figure 8c), confirming that the in-channel storage process, which is activated most often for links at capacity, is responsible for creating large temporal variability of bed sediment thickness. Furthermore, if we select those links for which the relative capacity RC_i^{final} is greater than 0.995 (shown in the inset of Figure 8c), we see that the magnitude of $dCOV_i$ is proportional to $\ell_i(B_i\ell_i + B_{u1}\ell_{u1} + B_{u2}\ell_{u2})$ (Figure 8d), which is the term that determines the strength of the feedback between the volume of sediment in storage and the resulting slope (related to the term in equation (5), the extra ℓ_i arises due to the conversion from bed elevation to slope via equation (6)).

Each link in the network was classified based on the temporal variability of its bed sediment thickness from the network, in-channel storage model and from the single link, in-channel storage model. Links with a $dCOV_i$ greater than a value of 0.2 (see dashed line in Figure 8b) are referred to as having a large variability or variability greater than Poisson and less than this value are referred to as having variability consistent with the Poisson distribution $\hat{f}\left(h_{s,i,t}\right)$ or as Poisson variability. Each link was then classified (Figure 8e) as follows: *Generator*—links for which both models showed variability greater than Poisson; *Propagator*—links for which the network model showed variability greater than Poisson but not so for the single-link model; *Unrealized*—links for which the single-link model showed variability greater than Poisson but not so for the network model; or *Poisson*—links for which both models showed Poisson variability. Note that the generators in Figure 8e are the locations at capacity shown in Figure 6c. Propagators are downstream of generators as these links are largely transmitting the structure of the supply from upstream. Links classified as unrealized are also generally downstream of generators where the structure of the supply from the upstream network has been altered in such a way to prevent the temporal variability of bed sediment thickness from becoming greater than Poisson.

An asymmetric distribution of bed sediment thickness about the mean (as seen in Figure 7f) arose wherever bed elevation returned to its initial value $\eta_{i,0}$. Thus, when the channel slope of this link returned to its initial value $S_{i,0}$ (Figure 9b), the bed sediment thickness did not decrease further, resulting in an asymmetry (Figure 9a). In-channel storage directly downstream of this link was not occurring, and for the sake of argument here this effect has been ignored. To show that this was, in fact, responsible for the asymmetry, we reran the simulation with an initial slope of $S_{i,0}/2$. By doing so, the bed first built up and increased its slope sufficient to pass the sediment supply. The bed ultimately built up to a level where fluctuations in bed elevation never returned to the initial bed elevation, and the result was that the bed sediment thickness became symmetric about the mean (Figures 9c and 9d). We also note that the pdf of bed sediment thickness remained heavy tailed and the periodicity of the time series was largely unaffected (Figure 9c).

As an example of how network structure and local channel characteristics can alter bed sediment thickness, we zoom down to show several time series of bed sediment thickness along a pathway with several comparatively large tributaries (Figure 10; see location and extent of area in Figure 8e). The trimodal

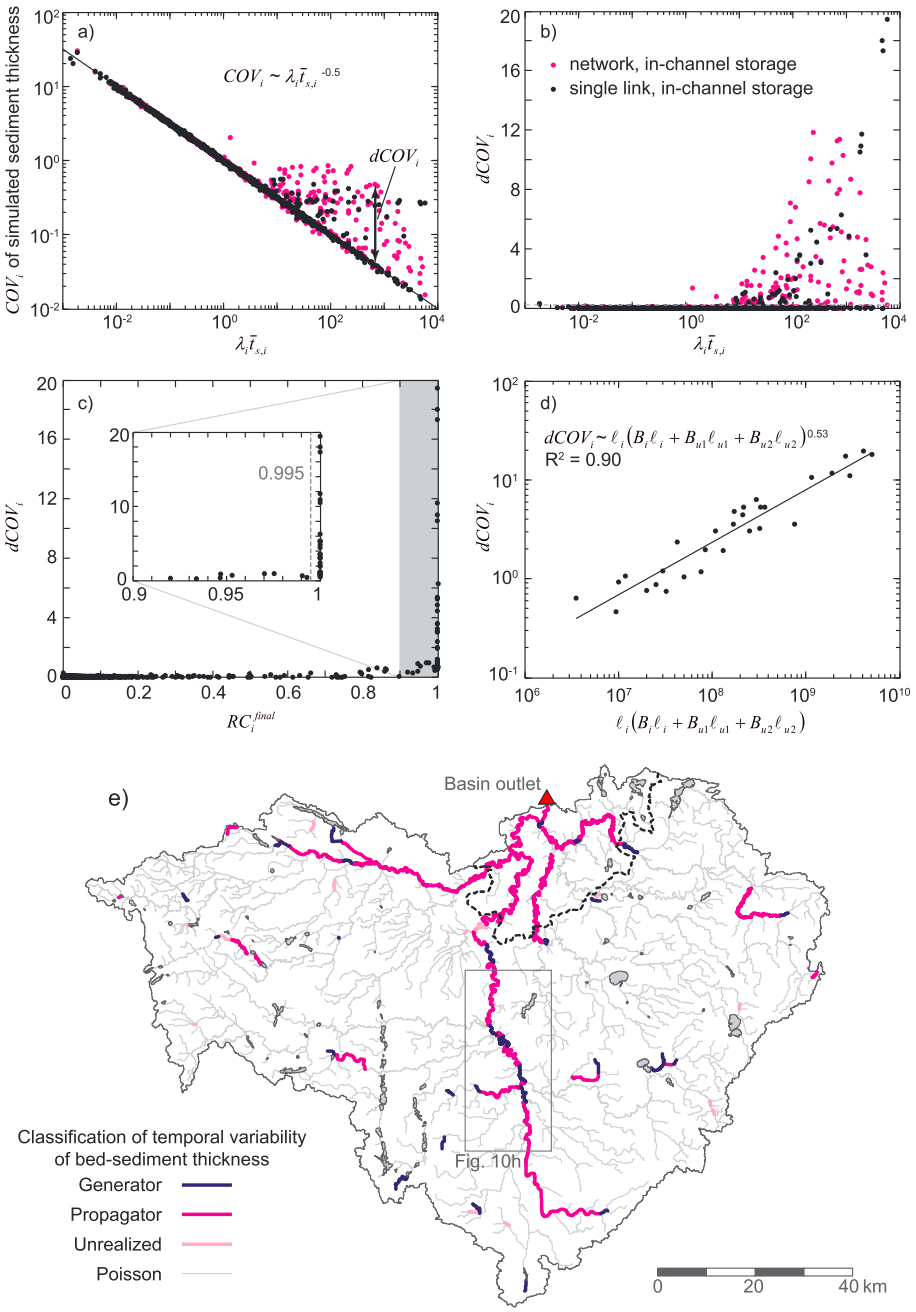

Figure 8. Controls on the temporal variability of simulated bed sediment thickness; insights from the single link, in-channel storage model (black) and the network, in-channel storage model (magenta). (a) The coefficient of variation COV_i of simulated bed sediment thickness versus the parameter of the Poisson distribution $\lambda_i \bar{t}_{s,i}$; note theoretical power law decay from equation (16). (b) The deviation $dCOV_i$ in Figure 8a from the theoretical power law decay. The gray dashed line at a value of 0.2 is marked as a threshold for classifying links in Figure 8e. (c) $dCOV_i$ versus relative capacity RC_i^{final}. Note that most of the deviation, i.e., the large temporal variability of bed sediment thickness greater than estimated from the Poisson distribution $\hat{f}(h_{s,i,t})$, occurs for links at capacity ($RC_i^{final} = 1$). (d) $dCOV_i$ versus the term $\ell_i(B_i\ell_i + B_{u1}\ell_{u1} + B_{u2}\ell_{u2})$ that determines the strength of the feedback between the volume of sediment in storage (placed within link i and two upstream links) and the resulting slope. Only those values from the single link, in-channel storage model where $RC_i^{final} > 0.995$ are shown. (e) Classification of temporal variability of bed sediment thickness as follows: *Generator*—links for which both models showed variability greater than Poisson (i.e., links with $dCOV_i > 0.2$); *Propagator*—links for which the network model showed variability greater than Poisson but not so for the single-link model; *Unrealized*—links for which the single-link model showed variability greater than Poisson but not so for the network model; or *Poisson*—links for which both models showed Poisson variability (i.e., links with $dCOV_i < 0.2$). Location and extent of Figure 10h is shown by a gray box. See text for definition of symbols.

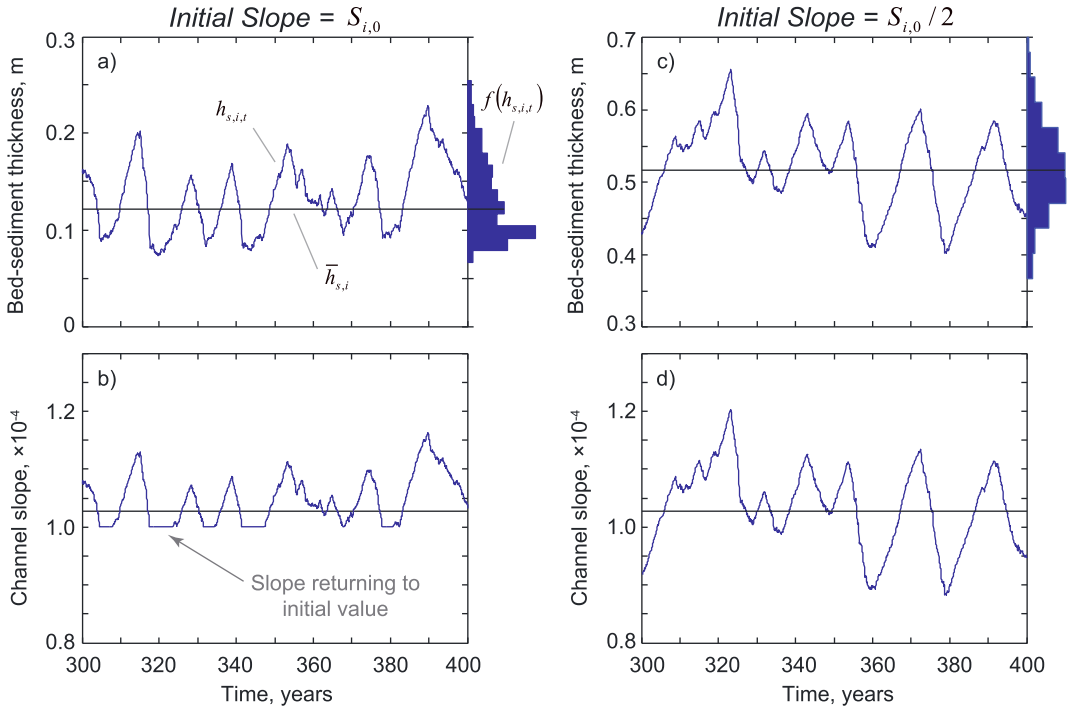

Figure 9. Links where the bed never builds up sufficiently and thus is constrained by the initial bed elevation have an asymmetric bed sediment thickness about the mean. The (a) bed sediment thickness and (b) channel slope under the same conditions as shown in Figure 7f; note the asymmetric distribution about the mean. The extent of the time series is shown from 300 to 400 years, but the probability distribution function $f(h_{s,i,t})$ of the bed sediment thickness (shown at the right) is computed from 200 to 600 years. The (c) bed sediment thickness and (d) channel slope for the same link but with half the initial slope, which allows the bed to build up sufficiently so fluctuations in bed elevation are not constrained by the initial bed elevation; note the symmetric distribution about the mean.

distribution $f(h_{s,i,t})$ of bed sediment thickness shown in Figure 7d (also shown in Figure 10a) arose due to the creation, alteration, and propagation of the structure of the sediment supplied from upstream. Just upstream of this link, we observed similar periodicity in bed sediment thickness but with a bimodal distribution (Figure 10b) and also the other directly upstream link had variability consistent with the Poisson distribution (classified as Poisson; see Figure 10h). The amalgamation and reprocessing of the bed material flux from these two upstream links gave rise to the trimodal distribution within the link shown in Figure 10a.

Even though only bed sediment thickness is shown in Figure 10, the difference between the flux in and flux out can be seen from the change in bed sediment thickness through time and, thus, when the flux from one link arrives in the directly downstream link. We generally observed that when the bed sediment thickness in a given link was at a local maximum, the bed sediment thickness in the directly downstream link was at a local minimum. This shows that when a link began to evacuate sediment, the downstream link began to accumulate that sediment (akin to sediment pulse movement described in *Gran and Czuba* [2017]). It is important to remember that the arrival of sediment to any one link was dictated by the supply from two directly upstream links and internal generation. Thus, the structure of the bed sediment thickness in one link did not necessarily directly translate into the structure of the bed sediment thickness in a directly downstream link. Although throughout many of the links shown in Figure 10, we observed that the underlying structure of the bed sediment thickness (e.g., periodicity) was largely translated downstream. This structure became altered progressing downstream depending on the relative magnitude of additional sediment supplied to the link (e.g., see Figures 10e–10g).

Another ubiquitous characteristic of bed sediment thickness, under transport-limited conditions or for affected links downstream, is periodicity. We quantified the dominant period T [T], for links with a $d\mathrm{COV}_i > 0.2$ (see Figure 8b), as the time period corresponding to the peak of the Fourier transform of simulated bed sediment thickness between 200 and 600 years and show this spatially for the single link,

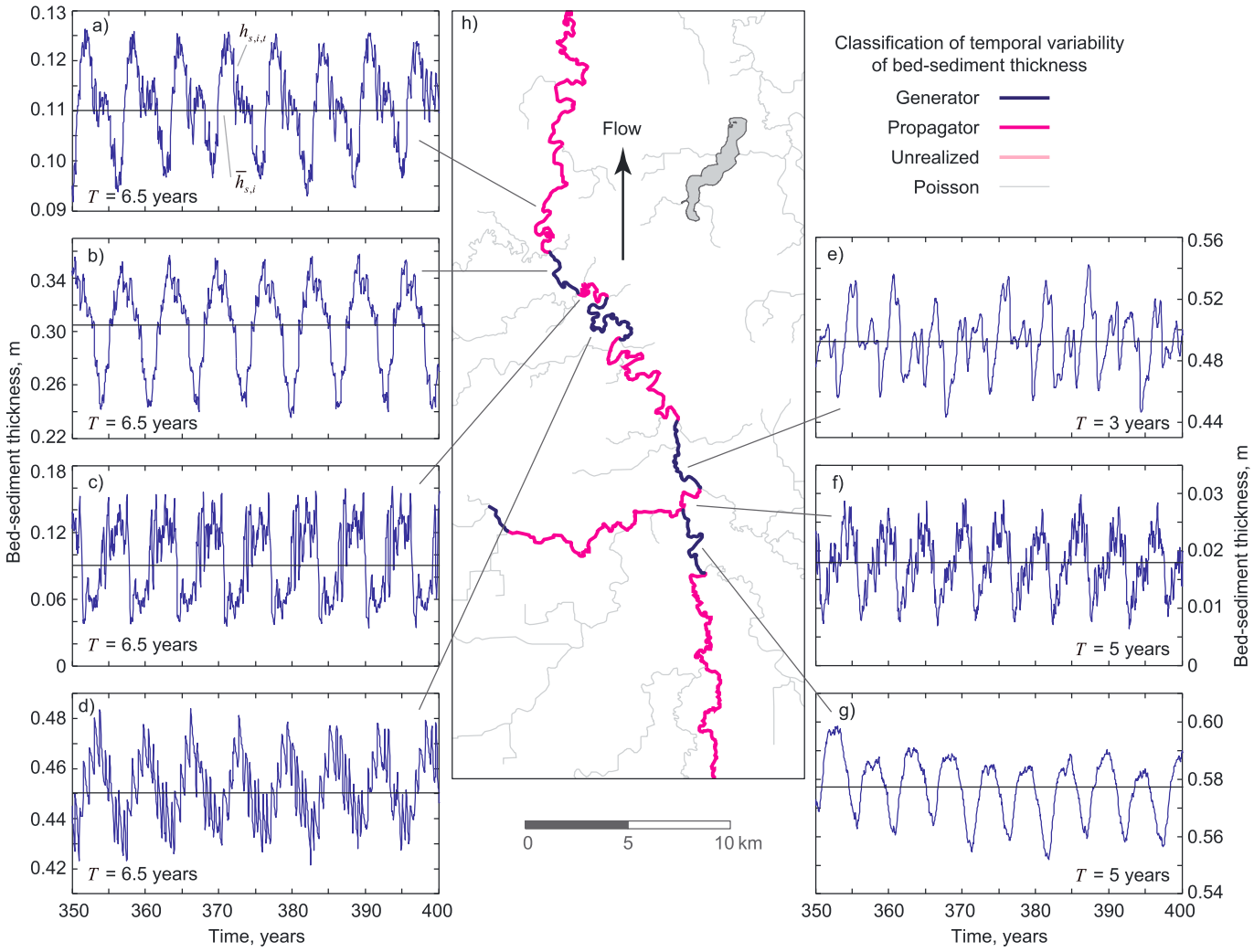

Figure 10. Propagation of the temporal structure of bed sediment thickness along the river network. (a–g) Time series of bed sediment thickness from 350 to 400 years. (h) The location of each time series. The trimodal distribution shown in Figure 7d is shown here in Figure 10a. The dominant period T of the bed sediment thickness time series is also indicated. See details on the link classification for Figure 10h in the text or in the caption of Figure 8.

in-channel storage model and the network, in-channel storage model (Figures 11a and 11b, respectively). We observed that the dominant period generally decreased downstream (Figure 11a) and decreased as the volumetric rate of sediment supply $V_p\lambda_i$ increased (Figure 11c). Even though we focus on the dominant period, it is important to note that multiple frequencies can be important. For instance, for the three time series shown in Figures 10e–10g, we computed their power spectra in Figure 11d. The two upstream links had dominant periods of 5 years, but the downstream link had a dominant period of 3 years. The period of 5 years was also present in the downstream link but due to the propagation, alteration, and amalgamation of the sediment inputs from upstream and generated internally, the period of 3 years arose and dominated this multiscale time series of bed sediment thickness.

5. Discussion

5.1. Key Insights

Heavy-tailed distributions of bed sediment thickness have been simulated in other network-based, bed material transport models with an in-channel storage component [*Benda and Dunne*, 1997a]. Knowing, or at least having a constraint on, the pdf of bed sediment thickness provides context for bed elevation fluctuations in response to sediment supply on whether the current bed elevation is part of expected fluctuations or

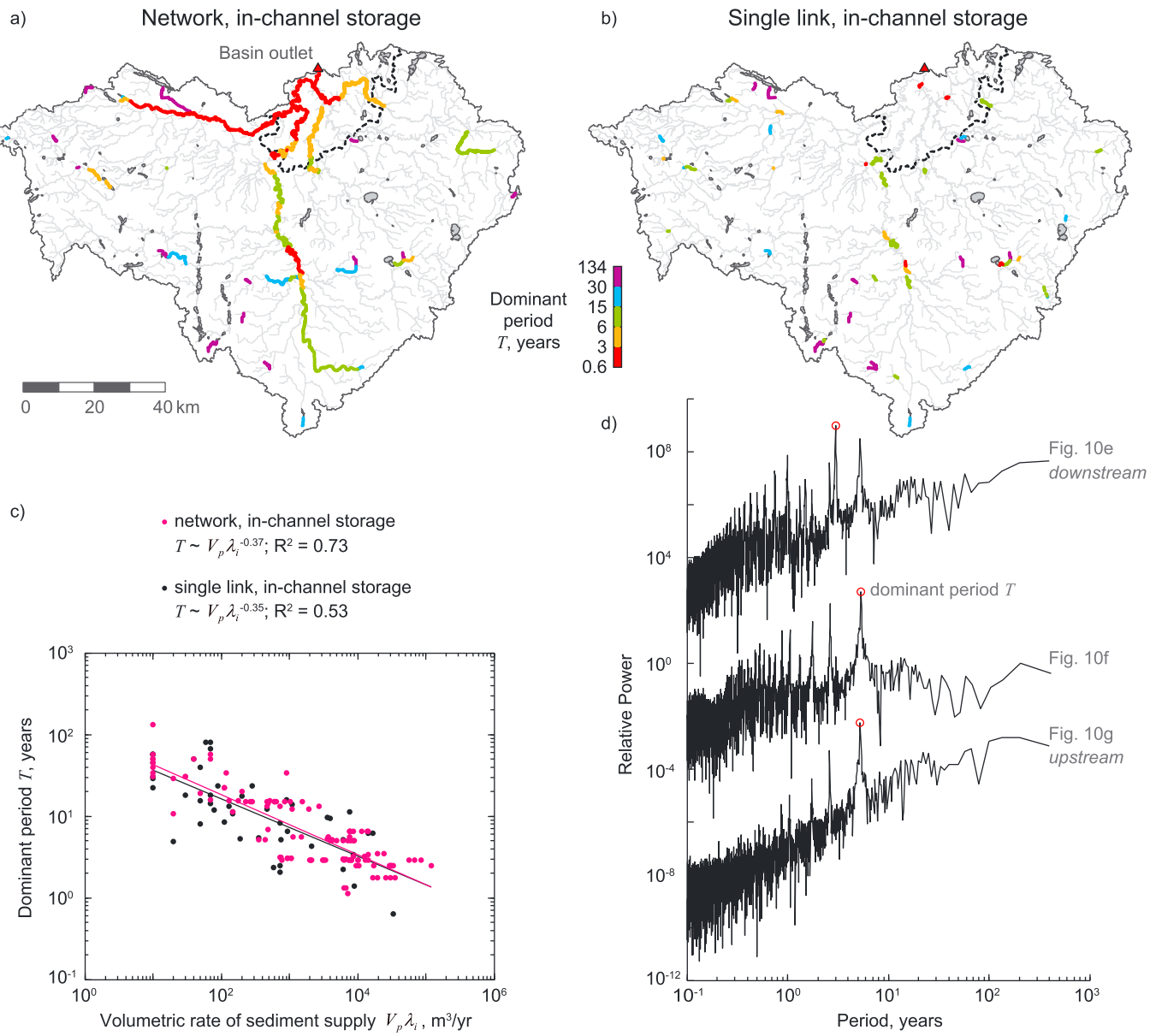

Figure 11. Periodicity of simulated bed sediment thickness arising from the buildup and release of sediment in storage. Spatial distribution of the dominant period T of simulated bed sediment thickness from the network, (a) in-channel storage model and the (b) single link, in-channel storage model. Only links with a $dCOV_i > 0.2$ (see Figure 8b) are shown. (c) The dominant period T decreases for increasing volumetric rate of sediment supply $V_p\lambda_i$. (d) The dominant period T was defined as the time period corresponding to the peak of the Fourier transform of simulated bed sediment thickness between 200 and 600 years (shown for the time series in Figures 10e–10g), although multiple frequencies can be important. Power spectra are arbitrarily vertically offset to make each spectrum visible.

cause for greater concern as a response to natural or human forcing. Large-scale fluctuations in bed elevation can affect infrastructure by undermining bridge piers, uncovering buried pipelines, or increasing flood risk.

The emergence of heavy tails in the pdf and periodicity in the time series of bed sediment thickness arose due to in-channel sediment storage and associated transport time delay. Whenever a reach approached at-capacity transport, then the in-channel storage dynamic became activated. It was for these reaches where we observed the largest fluctuations in bed sediment thickness compared to that estimated from a Poisson distribution (Figure 8c). The magnitude of these fluctuations depended upon the strength of the feedback between the volume of sediment placed in storage and the resulting bed slope (Figure 8d). Furthermore, the time series of bed sediment thickness for these reaches was periodic, with the dominant period decreasing downstream and with increasing volumetric supply rate of sediment. The volumetric supply rate

essentially sets how long it took to build up a given amount of sediment and thus how long it took to adjust the bed slope to a given level before evacuating the storage layer.

The most important aspect of this work is not in predicting the exact characteristics of the bed sediment thickness (e.g., mean, variance, pdf, and periodicity) but in illuminating some key insights on bed material sediment transport in river networks. Under supply-limited conditions, bed elevations may fluctuate in a predictable way according to the characteristics of the sediment supply (i.e., herein, we have related the pdf of bed sediment thickness directly to the characteristics of the sediment supply in equation (12)). We also see this effect in the model of *Benda and Dunne* [1997a] which showed first-order channels with bed sediment thickness (or sediment depth in their work) that closely varied with the supply from landslides and debris flows (with a periodic buildup and release; see their Figure 4). Progressing downstream the magnitude of the fluctuations in bed elevation relative to a mean bed elevation (or $COV_{i;}$ see Figure 8a) decrease because the sediment supply entering from an increasing number of tributaries leads to a more constant supply that is less sensitive to an input from an individual sediment-generating feature. This is essentially what is shown by *Benda and Dunne* [1997a] when looking at the distributions of bed sediment thickness in their Figure 5, and we have shown herein how this effect arises analytically. One caveat is that bed forms are ignored. Also, we see that a small change in channel slope (as the only morphodynamic degree of freedom in our model) allows for equilibrium transport akin to the assertion of *Ferguson et al.* [2015] that any increase in sediment supply is offset by an increase in transport capacity by changes in channel slope, morphology, or bed characteristics. Specifically, *Ferguson et al.* [2015] found that a small change in gravel texture was capable of sufficiently adjusting transport capacity to pass an increased sediment supply.

The emergence of periodicity in the time series of bed sediment thickness illustrates that there are factors inherent in the sediment-transport process (herein in-channel storage, but also in reality grain sorting and mixing and grain-size selective transport) [see *Parker*, 2008, and references therein] that can alter the structure of the arriving sediment supply before translating that sediment downstream. This means that there can be places within river networks, in the context of bed material sediment, that have the potential to shred signals in sediment supply [*Jerolmack and Paola*, 2010; *Van De Wiel and Coulthard*, 2010] and lead to the dispersion of sediment pulses [*Gran and Czuba*, 2017]. We were able to illustrate this effect in a transparent way with our relatively simple model. Perhaps more importantly, there can be a small fraction of reaches with relatively low-transport capacity within a nonequilibrium river network acting as bottlenecks that control or meter out sediment to downstream reaches. We have shown this in reaches at transport capacity (Figure 6) which alter the structure of bed sediment thickness, through the in-channel storage process, both locally (as generators in Figure 8) and downstream (giving rise to propagators in Figure 8) with large fluctuations and periodicity (Figure 11). In these cases, fluctuations in bed elevation can dissociate from signals in sediment supply. Therefore, downstream of these bottlenecks temporal variability in sediment supply cannot be inferred from the temporal variability of bed elevations. It remains to be further studied whether in graded, equilibrium river networks, signals in sediment supply can more effectively propagate downstream.

5.2. Model Limitations and Directions for Future Work

Fluctuations in bed elevation are inherent in the multiscale nature of sediment transport [e.g., *Singh et al.*, 2010, 2012], and at large scales, these fluctuations can indicate the movement of sediment pulses [see *Lisle*, 2008; *James*, 2010; *Gran and Czuba*, 2017, and references therein]. However, the regularity of the fluctuations in the time series of bed sediment thickness (i.e., periodicity) that arose from our present simulations is not something one should expect to see in the field. There were two major aspects of the model formulation that likely contributed to this regularity whereupon altering these aspects should give rise to seemingly more realistic fluctuations. The first aspect was the continuous long-term, probabilistic-average transport of sediment (i.e., specifying flow at a constant bankfull discharge with an associated intermittency factor) that averaged over the intermittent short periods with intense transport and long periods with low transport. Thus, even the "instantaneous" bed sediment thicknesses determined from the model inherently represented an average value. The second aspect was that sediment was supplied to the network randomly (each input delivered at a time independent from any others) following an exponential interarrival time distribution with a mean recurrence of 1 year. In reality, large amounts of sediment can be supplied across a region over a short duration due to heavy rainfall and high streamflows (violating the assumption of independent inputs) such that large magnitude inputs recur at a timescale much longer than 1 year (and

capturing the large-magnitude, low-frequency events may be an important supplier/driver of realistic bed material dynamics) [e.g., *Benda and Dunne*, 1997a, 1997b; *Istanbulluoglu et al*., 2004]. The present model averages over these potentially important factors of interannual variability that would likely give rise to a multiscale response in bed sediment thickness as pulses of sediment of various sizes transport and disperse throughout the network.

Supply-limited reaches underlain by bedrock or armored by a coarse lag would be expected to have an asymmetric temporal distribution of bed sediment thickness where a large fraction of time is spent with exposed bedrock or an armor layer. We see this in Figure 9 where a veneer of sediment (bed sediment thickness just less than 0.1 m when the slope returns to its initial profile) was moving over a nonerodible substrate (artificially imposed in the model) giving rise to the asymmetric distribution of bed sediment thickness. We also see this effect in simulations of *Benda and Dunne* [1997a] where first-order bedrock reaches spend a large fraction of time exposed until they are covered by sediment from simulated landslides and debris flows. In our simulations, we fixed the initial bed elevation and did not allow supply-limited conditions to incise the bed. However, a veneer of mobile alluvium over a nonerodible substrate may not be typical for most sand bed rivers and an investigation of incisional dynamics is warranted to understand how it might influence model behavior at network scales beyond our current findings.

We can speculate how incisional dynamics might influence our overall results and interpretation of network dynamics. In reaches where $RC_i^{final} << 1$ (Figure 6c), the slope was much steeper than required to pass the supply. These reaches would compensate by incising into their bed (unless underlain by bedrock or armored by a coarse lag and assuming incision would be the dominant mode of adjustment), lowering their slopes, and eventually attaining a slope sufficient to just pass the supply. Once this occurs, these reaches would also be near capacity and in our simulations would initiate in-channel storage dynamics and generate large fluctuations and periodicities in the time series of bed sediment thickness characteristic of this model formulation. If incisional dynamics were incorporated in the model, then it is likely that over a long enough time, sediment bottlenecks would disappear as the river network grades to an equilibrium state where every reach is at transport capacity and capable of passing the supply. This means that sediment bottlenecks are a characteristic of nonequilibrium river networks. Clearly, model simulations suggest that the Greater Blue Earth River Basin is still adjusting from Holocene glaciation.

Network-scale, bed material sediment routing models, such as the present model, are exceedingly difficult to verify against field measurements. Any measurements of bed sediment thickness will represent the value at an instant in time and not a true average over at least tens of years as would be consistent with our present model. In the field, the instantaneous bed sediment thickness would need to be averaged over a reach and the lower boundary (coarse lag deposits or bedrock) would need to be easily identified. The bed sediment thickness as defined in the model was somewhat arbitrarily set as the depth above an initial profile that is not necessarily at the level of a coarse lag or bedrock. More importantly, we recognize that channels may adjust transport capacity in more ways than we have represented in the model, specifically as adjustments in channel planform, geometry, and roughness. This makes the comparison difficult and explains why *Wilkinson et al*. [2006] compared their results to a simple mapping of the percentage of the bed covered by bed material. They essentially used a balance between supply rate to transport capacity to estimate an average bed sediment thickness (akin to our equation (13)). In their system, where bedrock exposure was common, they were able to correctly predict the presence or absence of bed material accumulation in 71% of mapped links. This provides us with some confidence that a balance between supply rate and transport capacity at the river-network scale can provide reasonable estimates of sediment accumulation even though we do not provide a validation of our own estimates. The model results are useful, nevertheless as indicators of locations in the channel network where channel adjustment (via slope or otherwise) is needed, possibly on a temporally varying basis, to transport the amount and type of sediment supplied by the available flow.

Even with confidence in the inputs and in the reach-scale transport dynamics, given the long timescales and large spatial scales of the model, it is very difficult to objectively test this type of model. One avenue for comparison is through residence-time distributions of sediment in a reach from simulations versus observations. Residence-time distributions are another emergent property that provide a common linkage from reach-scale dynamics to watershed-scale behavior and have received much attention in recent literature

[e.g., *Rinaldo et al*., 2015]. While not shown here, the residence-time distribution of bed material sediment in a link ranges from the travel time of sediment in a link $t_{s,i,t}$ to roughly the dominant period T in a link (as this sets the timescale when most sediment capable of being evacuated, would be evacuated from the in-channel storage reservoir). Perhaps in time, a detailed quantification of residence-time distributions from the field and numerical simulations that are then related to hydrogeomorphic properties will allow for suitable validation and ultimately lead to better parameterizations of reach-scale dynamics for incorporating into this or similar modeling framework. For now, we have focused on describing how this particular model formulation gives rise to the simulated behavior and also on isolating the role of the channel network on bed material dynamics. Different storage formulations may give rise to different emergent behavior, and as the use of network-based models become more widespread, it will be important to understand the connection between the specific formulation (including specification of inputs and mechanics of storage) and simulated behavior.

One major limitation of the present model is not accounting for channel-floodplain interactions that are important for accurately quantifying how sediment moves through a watershed. Thus, a logical next step is to implement a mechanism for sediment storage and release from floodplains. Developing a probabilistic approach to floodplain exchange is fairly straightforward given the channel migration rate and the sediment load for a given reach [e.g., *Malmon et al*., 2003; *Lauer and Willenbring*, 2010; *Viparelli et al*., 2013; *Lauer et al*., 2016]. The residence time of sediment in the floodplain is a key constraint for simulating channel-floodplain exchange. An understanding of floodplain residence time is beginning to emerge from an analysis of river-migration models [*Bradley and Tucker*, 2013] and from work that first measures the relevant fluxes and exchanges and then develops the mathematical foundations around these measurements to understand sediment delivery timescales [*Pizzuto*, 2012; *Pizzuto et al*., 2014]. But the component that is needed for network-scale models is a generalized understanding of the controls on floodplain residence time from floodplain, channel, sedimentologic, and hydrologic characteristics.

6. Summary

We have developed a network-based, bed material sediment routing model that combines spatially explicit sediment sourcing with in-channel transport and storage dynamics on a river network. The model was able to compute spatiotemporal changes in bed sediment thickness along an entire river network, elucidating how river networks organize and process sediment supply. We applied our model to sand transport in the agricultural Greater Blue Earth River Basin in Minnesota. The arrival of sediment to links of the network was cast as a Poisson process, and the model was used to simulate transport and storage dynamics over a 600 year time period. Properties of the Poisson arrival process allowed us to derive analytically (under supply-limited conditions) the time-averaged probability distribution function (pdf) of bed sediment thickness for each link of the river network for any spatial distribution of inputs. Under transport-limited conditions, the assumptions of the Poisson arrival process were violated due to in-channel storage dynamics that precluded an analytical derivation of the pdf of bed sediment thickness. Instead, we were able to (1) compute semianalytically the time-averaged bed sediment thickness and (2) provide a lower limit on the temporal variability of bed sediment thickness. This was accomplished by computing iteratively the bed slope adjustment required to pass the sediment supply, converting it to bed sediment thickness and then adding this to the analytically derived bed sediment thickness under supply-limited conditions.

The in-channel storage process was shown to alter the dynamic structure of the downstream sediment supply giving rise to large fluctuations and periodicity in the time series of bed sediment thickness. Large fluctuations in bed sediment thickness arose from reaches transporting at capacity and the magnitude of those fluctuations depended upon the strength of the feedback between the volume of sediment placed in storage and the resulting bed slope. Additionally, periodicities in bed sediment thickness arose in these reaches, with the dominant period decreasing downstream and with increasing volumetric supply rate of sediment. The volumetric supply rate essentially sets how long it took to build up a given amount of sediment and thus how long it took to adjust the slope to a given level before evacuating the storage layer.

Using the developed model, we were able to extract some key insights on bed material sediment transport in river networks. Under supply-limited conditions, bed elevations fluctuated in a predictable way according to the characteristics of the sediment supply. Progressing downstream, increased convergence of tributaries

rendered the sediment supply less sensitive to individual sediment-generating features and thus reduced the variability of bed elevation fluctuations, ignoring bed forms which were not included in this model. Also, it was shown that a small fraction of reaches with relatively low transport capacity within a nonequilibrium river network can emerge, acting as bottlenecks that control or meter out sediment to downstream reaches. In these cases, fluctuations in bed elevation can dissociate from signals in sediment supply. Therefore, downstream of these bottlenecks temporal variability in sediment supply cannot be inferred from the temporal variability of bed elevations. As a river network grades to an equilibrium state, the influence of sediment bottlenecks would likely disappear and it remains to be further studied how bed sediment dynamics of the whole system would reorganize in response.

Appendix A: Selecting a Characteristic Vertical Length Scale for Sand Transport

The characteristic vertical length scale for sand transport ($\theta_i H_i$) is set by θ_i which defines a fraction of the flow depth below which the majority of sand transport takes place. The majority can be defined quantitatively as capturing a certain percentage of the total sand load, which can be calculated as the product of the vertical distributions of suspended sediment and velocity. This analysis is specific to a single link *i* and for simplicity the index *i* has been dropped.

The Rouse-Vanoni-Ippen suspended-sediment distribution [*Garcia*, 2008] is given by

$$\frac{\overline{c}}{\overline{c}_b} = \left[\frac{(H-z)/z}{(H-b)/b}\right]^{Z_R}, \tag{A1}$$

where $\overline{c}$ [ML^3] is the suspended-sediment concentration averaged over turbulence at a distance z above the bed, $\overline{c}_b$ [ML^3] is the near-bed suspended-sediment concentration averaged over turbulence, H [L] is the flow depth, z [L] is the distance above the bed, b [L] is the near-bed distance above the bed, and Z_R is the dimensionless Rouse number given as

$$Z_R = \frac{v_s}{\kappa u^*}, \tag{A2}$$

where v_s [LT^{-1}] is the sediment fall velocity, $\kappa = 0.41$ is the von Karman's constant, and u^* [LT^{-1}] is the shear velocity. Sediment fall velocity was computed from the empirical relation of *Dietrich* [1982] as

$$R_f = \exp\left\{-b_1 + b_2 \ln\left(R_{ep}\right) - b_3\left[\ln\left(R_{ep}\right)\right]^2 - b_4\left[\ln\left(R_{ep}\right)\right]^3 + b_5\left[\ln\left(R_{ep}\right)\right]^4\right\}, \tag{A3}$$

where R_f is a dimensionless fall velocity

$$R_f = \frac{v_s}{\sqrt{gRD}}, \tag{A4}$$

$g = 9.81$ m s^{-2} [LT^2] is the acceleration due to gravity, $R = 1.65$ is the submerged specific gravity of sediment, D [L] is the sediment grain size, R_{ep} is a dimensionless particle Reynolds number

$$R_{ep} = \frac{v_s D}{\nu}, \tag{A5}$$

$\nu = 1 \times 10^{-6}$ m^2 s^{-1} [L^2T] is the kinematic viscosity of water, and the coefficients are given as $b_1 = 2.891394$, $b_2 = 0.95296$, $b_3 = 0.056835$, $b_4 = 0.002892$, and $b_5 = 0.000245$ (as presented by *Garcia* [2008]). The shear velocity was calculated via the depth-slope product for the bed shear stress as

$$u^* = \sqrt{gHS}, \tag{A6}$$

where S is the channel slope. For convenience, equation (A1) can be rearranged as

$$\frac{\overline{c}}{\overline{c}_b} = \left[\frac{\left(\frac{1}{z/H} - 1\right)}{\left(\frac{1}{b/H} - 1\right)}\right]^{Z_R}, \tag{A7}$$

which relates the relative concentration $\overline{c}/\overline{c}_b$ to the relative depth z/H where $b/H = 0.05$ [*Vanoni*, 1975].

The velocity distribution according to *Keulegan* [1938] is given by

$$\frac{u}{u^*} = \frac{1}{\kappa} \ln\left(30\frac{z}{k_s}\right), \tag{A8}$$

where u [LT^{-1}] is the time-averaged flow velocity at a distance z above the bed and $k_s = 2D$ [L] is an effective roughness height [*Garcia*, 2008]. Rearranging, we can write equation (A8) as

$$\frac{u}{u^*} = \frac{1}{\kappa} \ln\left[30\frac{(z/H)}{(k_s/H)}\right], \tag{A9}$$

which relates the relative velocity u/u^* to the relative depth z/H.

In multiplying equation (A7) by equation (A9), we can compute a vertical distribution of the relative suspended-sediment load and take the cumulative sum of this distribution from the bed. Then θ_i can be computed directly from the cumulative distribution of relative suspended-sediment load (normalized so the maximum of the cumulative distribution is equal to one) as the vertical location which captures a certain percentage of the suspended-sediment load. Note that only the relative distributions are necessary and not the actual distributions because we only need to know, in a relative sense, how much sediment is transported at various points throughout the water column.

For the study basin at the 2 year recurrence interval flow and where $D = 0.4$ mm, the value of $\theta_i = 0.1$ captures 73% of the total sand load on average for all links of the network (standard deviation of 18%). Similarly, say we wanted θ_i to capture 80% of the total sand load, then on average $\theta_i = 0.15$ (standard deviation of 0.1), or for 90%, then on average $\theta_i = 0.23$ (standard deviation of 0.14). Herein, we maintain $\theta_i = 0.1$ for all links.

Appendix B: Iterative Procedure for Calculating the Time-Averaged Thickness of the Storage Layer

Herein, we describe an iterative procedure for calculating $\overline{h}_{s,i}^{stor}$ by adjusting channel slope until every reach was capable of transporting its supply. This procedure is only for calculating $\overline{h}_{s,i}^{stor}$ and is independent of the model simulations which simulate $h_{s,i,t}$ and the buildup of sediment within in-channel storage directly.

First, we compute the relative capacity RC_i^{iter} of a given link i to transport sediment, where iter denotes the current iteration, by comparing the rate of sediment supply to the rate of sediment transport as

$$RC_i^{iter} = \frac{V_p \lambda_i \tilde{t}_{s,i}^{iter}}{\ell_i(\theta_i H_i) B_i}, \tag{B1}$$

where $\tilde{t}_{s,i}^{iter}$ [T] is the travel time for a sand parcel to move through a given link i that is iterated upon, as the "~" denotes an iterated value. The component of $\tilde{t}_{s,i}^{iter}$ via equation (1) that is iterated upon is the slope $\tilde{S}_i^{iter}$ and for the first iteration $\tilde{S}_i^1$ is the initial slope $S_{i,0}$. The links where $RC_i^{iter} > 1$ will ultimately aggrade, so this identifies the channels that must adjust their slopes to pass the supply. This means that the volumetric transport rate of sand must adjust to balance the supply rate as

$$\frac{\ell_i(\theta_i H_i) B_i}{t_{s,i}^*} = V_p \lambda_i, \tag{B2}$$

where $t_{s,i}^*$ [T] is the travel time for a sand parcel to move through a given link when transport balances supply, as the superscript "*" denotes a value computed when transport balances supply. The channel slope S_i^* that a link must adjust to in order to pass the sediment supply is given by substituting equation (1) into equation (B2) and rearranging as

$$S_i^* = \left(\frac{V_p \lambda_i g^{1/2} R_i^2 D_i}{0.05 B_i u_{w,i}^2 H_i^{3/2}}\right)^{2/3}. \tag{B3}$$

Thus wherever $RC_i^{iter} > 1$, the elevation $\tilde{\eta}_i^{iter}$ [L] at the upstream end of the link must increase to achieve a slope of S_i^* as

$$\tilde{\eta}_i^{iter+1} = \tilde{\eta}_i^{iter} + \ell_i\left(S_i^* - \tilde{S}_i^{iter}\right), \tag{B4}$$

and for the first iteration $\widetilde{\eta}_i^1$ is the initial bed elevation $\eta_{i,0}$. Once all of the elevations have been adjusted for all links above transport capacity to $\widetilde{\eta}_i^{\text{iter}+1}$, then channel slope can be recomputed for the entire network via equation (6) to $\widetilde{S}_i^{\text{iter}+1}$. An increase in slope in one link simultaneously decreases the slope in the directly upstream links, and because the subsequent decrease in slope may put that link above transport capacity, we have to iterate this procedure until $\text{RC}_i^{\text{final}} \leq 1$. It is important to note that for links that have adjusted their slopes following this procedure, one must use the final iterated value for $\widetilde{t}_{s,i}^{\text{final}}$ (via $\widetilde{S}_i^{\text{final}}$) for $\overline{t}_{s,i}$ in order to accurately compute $f\left(h_{s,i,t}^{\text{act}}\right)$ via equation (12) and $\overline{h}_{s,i}^{\text{act}}$ via equation (13) in the context of in-channel storage.

In the formulation described herein, the same storage volume is reported both as bed elevation (for updating slopes) and as bed sediment thickness (for conveniently reporting the volume of sediment in a link). When this volume is reported as a bed elevation, we have conceptually placed that volume in three wedges (one in link *i* and the other two in upstream links; Figure 2b), but when we report that same storage volume as a bed sediment thickness, we have conceptually placed the entirety of that storage volume uniformly across the bed of link *i* (Figure 2a). Through this iterative procedure we have calculated an adjusted bed elevation at which all links are capable of transporting the supply $\widetilde{\eta}_i^{\text{final}}$ that we now need to convert to the time-averaged thickness of the storage layer $\overline{h}_{s,i}^{\text{stor}}$ as

$$\overline{h}_{s,i}^{\text{stor}} = \frac{\left(\widetilde{\eta}_i^{\text{final}} - \eta_{i,0}\right)\left(B_i\ell_i + B_{u1}\ell_{u1} + B_{u2}\ell_{u2}\right)}{2B_i\ell_i}. \tag{B5}$$

Appendix C: Sand Inputs From Bluffs, Ravines, and Uplands

C1. Bluffs

Bluffs were defined in this basin by *Belmont et al.* [2011] as areas along active channels that had greater than 3 m of relief within a 9 m × 9 m moving window (Figure 4). Bluffs in the Greater Blue Earth River Basin are as tall as 70 m and flank roughly 50% of the active-channel corridor within the knickzone. Bluffs separated from the river channel by terraces were excluded from the sediment source inventory. Nearly 3500 individual bluffs were mapped from 3 m lidar data in the Greater Blue Earth River Basin. According to the sediment budget [*Gran et al.*, 2011; *Belmont et al.*, 2011; *Bevis*, 2015], the mass erosion rate of sand from each bluff ($M_{s,b}$ [MT^{-1}] in Mg yr^{-1}, where the subscript *b* denotes a bluff) was calculated as

$$M_{s,b} = e_b A_b f_{s,\text{till}} \rho_{\text{till}}, \tag{C1}$$

where e_b [LT^{-1}] is the long-term, subbasin-averaged bluff erosion rate in m yr^{-1} (ranging from 0.05 to 0.25 m yr^{-1}) determined through repeat aerial photo analysis of bluff crests between 1938 and 2005 or 2008 as described in *Day et al.* [2013b] and *Bevis* [2015], A_b [L^2] is the individual bluff surface area projected onto a vertical plane in m^2, $f_{s,\text{till}}$ is the fraction of sand in the till (0.35), and ρ_{till} [ML^{-3}] is the average bulk density of the till (1.8 Mg m^{-3}). Even though all bluffs are not composed of till, we treat them as such with minimal error. The total mass erosion rate of sand from all bluffs in the Greater Blue Earth River Basin was computed as 2.7×10^5 Mg yr^{-1} and was spatially distributed according to Figure 5a.

C2. Ravines

Ravines were defined in this basin by *Belmont et al.* [2011] as steep, ephemerally flowing channels that connect the low-gradient uplands to deeply incised valleys (Figure 4). Ravines deliver most of their sediment load during high-magnitude precipitation events before crops are fully established in spring and early summer and are often dry by late summer. Nearly 340 individual ravines were mapped from 3 m lidar data in the Greater Blue Earth River Basin. Field monitoring of five ravines in the lower Le Sueur River Basin as part of the sediment budgeting work by *Belmont et al.* [2011] was used to determine an average annual ravine yield. According to the sediment budget [*Gran et al.*, 2011; *Belmont et al.*, 2011; *Bevis*, 2015], the mass erosion rate of sand from each ravine ($M_{s,r}$ [MT^{-1}] in Mg yr^{-1}, where the subscript *r* denotes a ravine) was calculated as

$$M_{s,r} = A_r Y_r f_{s,\text{till}}, \tag{C2}$$

where A_r [L^2] is the incised area of an individual ravine in m^2 and Y_r [$\text{ML}^2\ \text{T}^{-1}$] is the average annual ravine yield (3.4×10^{-3} Mg m^{-2} yr^{-1}) set as a constant for all ravines. Not all ravines incise through till but are

treated as such with minimal error. The total mass erosion rate of sand from all ravines in the Greater Blue Earth River Basin was computed as 2.4×10^4 Mg yr^{-1} and was spatially distributed according to Figure 5b.

C3. Uplands

Uplands contribute sediment primarily from agricultural fields. Each link has a corresponding upland area for a total of 1360 upland areas. An analysis of total suspended solids data measured at two gages upstream of the knickzone in the Le Sueur River Basin combined with sediment fingerprinting as part of the sediment budgeting work by *Belmont et al.* [2011] was used to determine an average annual upland yield. According to the sediment budget [*Gran et al.*, 2011; *Belmont et al.*, 2011; *Bevis*, 2015], the mass erosion rate of sand from each upland area ($M_{s,u}$ [MT^{-1}] in Mg yr^{-1}, where the subscript u denotes an upland) was calculated as

$$M_{s,u} = a_i Y_u f_{s,\mathrm{soil}}, \tag{C3}$$

where a_i is the upland area or incremental contributing area to link i in m^2, Y_u [ML^2 T^{-1}] is the annual upland yield (2×10^{-5} Mg m^{-2} yr^{-1}) set as a constant for all uplands, and $f_{s,\mathrm{soil}}$ is the fraction of sand in the soil (0.10 for glaciolacustrine deposits, 0.35 for glacial till, or 0.50 for glacial outwash and Holocene alluvium) [*STATSGO2*, 2015] (see Figure 5c). The total mass erosion rate of sand from all uplands in the Greater Blue Earth River Basin was computed as 5.7×10^4 Mg yr^{-1} and was spatially distributed according to Figure 5c. Note that the extent of glaciolacustrine deposits reflects the approximate historical extent of glacial Lake Minnesota.

Notation

a_i	directly contributing area of link i [L^2];
A_b	bluff surface area projected onto a vertical plane [L^2];
A_i	upstream drainage area of link i [L^2];
A_r	incised area of a ravine [L^2];
b	near-bed distance above the bed [L];
b_1, b_2, b_3, b_4, and b_5	coefficients of the sediment fall velocity relation of *Dietrich* [1982] as presented by *Garcia* [2008];
B_i	channel width of link i [L];
$\overline{c}$	suspended-sediment concentration averaged over turbulence at a distance z above the bed [ML^3];
$\overline{c}_b$	near-bed suspended-sediment concentration averaged over turbulence [ML^3];
COV_i	coefficient of variation;
d	index of the link directly downstream of link i;
$d\mathrm{COV}_i$	deviation of the COV_i from that predicted for a Poisson distribution;
D_i	sediment grain size in link i [L];
e_b	long-term, subbasin-average bluff erosion rate [LT^{-1}];
$f_{s,\mathrm{soil}}$	fraction of sand in soil;
$f_{s,\mathrm{till}}$	fraction of sand in till;
$f(h_{s,i,t})$	probability distribution function of $h_{s,i,t}$;
$\hat{f}\left(h_{s,i,t}\right)$	estimate of $f(h_{s,i,t})$ assuming the in-channel storage process preserves the structure of a Poisson arrival process;
$f\left(h_{s,i,t}^{\mathrm{act}}\right)$	probability distribution function of $h_{s,i,t}^{\mathrm{act}}$;
$f\left(k;\lambda_i \overline{t}_{s,i}\right)$	Poisson distribution with index k and parameter $\lambda_i \overline{t}_{s,i}$;
g	acceleration due to gravity [LT^{-2}];
$\overline{h}_{s,i}$	time-averaged bed sediment thickness of link i [L];
$\overline{h}_{s,i}^{\mathrm{act}}$	time-averaged bed sediment thickness of the active-transport layer of link i [L];
$\overline{h}_{s,i}^{\mathrm{stor}}$	time-averaged bed sediment thickness of the storage layer of link i [L];
$h_{s,i,t}$	bed sediment thickness of link i at time t [L];
$h_{s,i,t}^{\mathrm{act}}$	bed sediment thickness of the active-transport layer of link i at time t [L];
$h_{s,i,t}^{\mathrm{stor}}$	bed sediment thickness of the storage layer of link i at time t [L];

H_i flow depth of link i [L];
$H_{s,i}$ thickness of the active-transport layer at capacity of link i [L];
i link index;
iter index of the current iteration;
$I_{f,s}$ intermittency factor for sand transport;
k index of Poisson distribution;
k_s effective roughness height [L];
ℓ_i length of link i [L];
$M_{s,b}$ mass erosion rate of sand from a bluff [MT^{-1}];
$M_{s,r}$ mass erosion rate of sand from a ravine [MT^{-1}];
$M_{s,u}$ mass erosion rate of sand from an upland area [MT^{-1}];
n_i total number of inputs of volume V_p upstream of link i but downstream of any lakes directly connected to the network;
N_i number of parcels within link i for duration $\bar{t}_{s,i}$;
R_{ep} dimensionless particle Reynolds number;
R_f dimensionless fall velocity;
R_i submerged specific gravity of sediment in link i;
RC_i^{iter} relative capacity of link i at iteration iter;
$\tilde{S}_i^{iter}$ iterated channel slope of link i at iteration iter;
S_i^* channel slope of link i where sediment transport equals supply;
$S_{i,t}$ channel slope of link i at time t;
t time index;
$\bar{t}_{s,i}$ time-averaged travel time of a sand parcel through link i [T];
$\tilde{t}_{s,i}^{iter}$ iterated travel time of a sand parcel through link i at iteration iter [T];
$t_{s,i}^*$ travel time of a sand parcel through link i when sediment transport equals supply [T];
$t_{s,i,t}$ travel time of a sand parcel through link i at time t [T];
T dominant period of $h_{s,i,t}$ [T];
u time-averaged flow velocity at a distance z above the bed [LT^{-1}];
$u1$, $u2$ indices of directly upstream channel links;
u^* shear velocity [LT^{-1}];
$u_{w,i}$ streamflow velocity in link i [LT^{-1}];
V_p parcel volume [L^3];
$V_{s,i,t}$ total volume of sand from all parcels in link i at time t [L^3];
$V_{s,i,t}^{stor}$ total volume of sand in storage in link i at time t [L^3];
Y_r average annual ravine yield [ML^2T^{-1}];
Y_u annual upland yield [ML^2T^{-1}];
z distance above the bed [L];
Z_r dimensionless Rouse number;
α_{HA} coefficient of the $H_i \sim A_i$ scaling relation;
α_{u_wA} coefficient of the $u_{w,i} \sim A_i$ scaling relation;
β_{HA} exponent of the $H_i \sim A_i$ scaling relation;
β_{u_wA} exponent of the $u_{w,i} \sim A_i$ scaling relation;
$\tilde{\eta}_i^{iter}$ iterated bed elevation at the upstream end of link i at iteration iter [L];
$\eta_{i,t}$ bed elevation at the upstream end of link i at time t [L];
θ_i scale factor for determining the characteristic vertical length scale for sand transport in link i;
κ von Karman's constant;
λ rate parameter of the exponential interarrival time distribution [T^{-1}];
λ_i rate of Poisson arrivals to link i [T^{-1}];
ν kinematic viscosity of water [L^2 T];
v_s sediment fall velocity [LT^{-1}];

ρ_s sediment density [ML^{-3}];
ρ_{till} average bulk density of till [ML^{-3}];
$\sigma_{h_s,i}$ standard deviation of $h_{s,i,t}$ [L];
ϕ porosity of bed material sediment;
χ_i volume of the active-transport layer at capacity of link i [L^3].

Acknowledgments
This research was funded by NSF grant EAR-1209402 under the Water Sustainability and Climate Program (WSC): REACH (REsilience under Accelerated CHange) and benefited from collaborations made possible by NSF grant EAR-1242458 under Science Across Virtual Institutes (SAVI): LIFE (Linked Institutions for Future Earth). J.A.C. acknowledges support provided by an Interdisciplinary Doctoral Fellowship through the University of Minnesota Graduate School and Institute on the Environment and also an Edward Silberman Fellowship through the St. Anthony Falls Laboratory. We thank two anonymous reviewers, the Associate Editor (Joel Johnson), and Editor (John Buffington) for comments that helped improve the presentation, sharpen the focus, and distill the broader implications of our work. The sediment budget data for the Greater Blue Earth River Basin are available from *Bevis* [2015]. All model codes have been made freely available in the Community Surface Dynamics Modeling System (CSDMS) under the model heading "River Network Bed-Material Sediment" (http://csdms.colorado.edu/wiki/Model:River_Network_Bed-Material_Sediment).

References

Belmont, P., et al. (2011), Large shift in source of fine sediment in the upper Mississippi River, *Environ. Sci. Technol.*, *45*, 8804–8810, doi:10.1021/es2019109.
Belmont, P. (2011), Floodplain width adjustments in response to rapid base level fall and knickpoint migration, *Geomorphology*, *128*(1–2), 92–102, doi:10.1016/j.geomorph.2010.12.026.
Benda, L., and T. Dunne (1997a), Stochastic forcing of sediment routing and storage in channel networks, *Water Resour. Res.*, *33*(12), 2865–2880, doi:10.1029/97WR02387.
Benda, L., and T. Dunne (1997b), Stochastic forcing of sediment supply to channel networks from landsliding and debris flow, *Water Resour. Res.*, *33*(12), 2849–2863, doi:10.1029/97WR02388.
Bevis, M. (2015), Sediment budgets indicate Pleistocene base level fall drives erosion in Minnesota's Greater Blue Earth River basin, MS thesis, Univ. of Minnesota Duluth.
Blann, K. L., J. L. Anderson, G. R. Sands, and B. Vondracek (2009), Effects of agricultural drainage on aquatic ecosystems: A review, *Crit. Rev. Environ. Sci. Technol.*, *39*(11), 909–1001, doi:10.1080/10643380801977966.
Bradley, D. N., and G. E. Tucker (2013), The storage time, age, and erosion hazard of laterally accreted sediment on the floodplain of a simulated meandering river, *J. Geophys. Res. Earth Surf.*, *118*, 1308–1319, doi:10.1002/jgrf.20083.
Bridge, J. S., and M. R. Leeder (1979), A simulation model of alluvial stratigraphy, *Sedimentology*, *26*(5), 617–644, doi:10.1111/j.1365-3091.1979.tb00935.x.
Brown, C. B. (1943), Discussion of sedimentation in reservoirs, *Proc. Am. Soc. Civ. Eng.*, *69*, 1493–1500.
Carlisle, D. M., M. R. Meador, T. M. Short, C. M. Tate, M. E. Gurtz, W. L. Bryant, J. A. Falcone, and M. D. Woodside (2013), The quality of our Nation's waters—Ecological health in the Nation's streams, 1993–2005, *U.S. Geol. Surv. Circ.*, *1391*, 120.
Clayton, L., and S. R. Moran (1982), Chronology of late Wisconsinan glaciation in middle North America, *Quat. Sci. Rev.*, *1*, 55–82.
Czuba, J. A., and E. Foufoula-Georgiou (2014), A network-based framework for identifying potential synchronizations and amplifications of sediment delivery in river basins, *Water Resour. Res.*, *50*, 3826–3851, doi:10.1002/2013WR014227.
Czuba, J. A., and E. Foufoula-Georgiou (2015), Dynamic connectivity in a fluvial network for identifying hotspots of geomorphic change, *Water Resour. Res.*, *51*, 1401–1421, doi:10.1002/2014WR016139.
Dadaser-Celik, F., and H. G. Stefan (2009), Stream flow response to climate in Minnesota, project report no. 510, 118 p., St. Anthony Falls Lab., Univ. of Minnesota, Minneapolis, Minn.
Day, S. S., K. B. Gran, P. Belmont, and T. Wawrzyniec (2013a), Measuring bluff erosion part 1: Terrestrial laser scanning methods for change detection, *Earth Surf. Process. Landforms*, *38*(10), 1055–1067, doi:10.1002/esp.3353.
Day, S. S., K. B. Gran, P. Belmont, and T. Wawrzyniec (2013b), Measuring bluff erosion part 2: Pairing aerial photographs and terrestrial laser scanning to create a watershed scale sediment budget, *Earth Surf. Process. Landforms*, *38*(10), 1068–1082, doi:10.1002/esp.3359.
Dietrich, W. E., J. W. Kirchner, H. Ikeda, and F. Iseya (1989), Sediment supply and the development of the coarse surface layer in gravel-bedded rivers, *Nature*, *340*, 215–217, doi:10.1038/340215a0.
Dietrich, W. E. (1982), Settling velocity of natural particles, *Water Resour. Res.*, *18*(6), 1615–1626, doi:10.1029/WR018i006p01615.
Durrett, R. (2012), *Essentials of Stochastic Processes*, p. 265, Springer, New York.
Engelund, F., and E. Hansen (1967), *A Monograph on Sediment Transport in Alluvial Streams*, p. 62, Tek. Forlag, Copenhagen, Denmark.
Ferguson, R. I., M. Church, C. D. Rennie, and J. G. Venditti (2015), Reconstructing a sediment pulse: Modeling the effect of placer mining on Fraser River, Canada, *J. Geophys. Res. Earth Surf.*, *120*, 1436–1454, doi:10.1002/2015JF003491.
Foufoula-Georgiou, E., Z. Takbiri, J. A. Czuba, and J. Schwenk (2015), The change of nature and the nature of change in agricultural landscapes: Hydrologic regime shifts modulate ecological transitions, *Water Resour. Res.*, *51*, 6649–6671, doi:10.1002/2015WR017637.
Garcia, M. H. (2008), Sediment transport and morphodynamics, in *Sedimentation Engineering: Processes, Measurements, Modeling, and Practice: ASCE Manuals and Reports on Engineering Practice*, vol. 110, edited by M. H. Garcia, pp. 21–163, ASCE, Reston, Va.
Gassman, P. W., M. R. Reyes, C. H. Green, and J. G. Arnold (2007), The soil and water assessment tool: Historical development, applications, and future research directions, *Trans. Am. Soc. Agric. Biol. Eng.*, *50*(4), 1211–1250.
Gran, K. G., and J. A. Czuba (2017), Sediment pulse evolution and the role of network structure, *Geomorphology*, *277*, 17–30, doi:10.1016/j.geomorph.2015.12.015.
Gran, K. B., N. Finnegan, A. L. Johnson, P. Belmont, C. Wittkop, and T. Rittenour (2013), Landscape evolution, valley excavation, and terrace development following abrupt postglacial base-level fall, *GSA Bull.*, *125*(11–12), 1851–1864, doi:10.1130/B30772.1.
Gran, K. B., P. Belmont, S. S. Day, C. Jennings, A. Johnson, L. Perg, and P. R. Wilcock (2009), Geomorphic evolution of the Le Sueur River, Minnesota, USA, and implications for current sediment loading, in *Management and Restoration of Fluvial Systems with Broad Historical Changes and Human Impacts*, vol. 451, edited by L. A. James, S. L. Rathburn, and G. R. Whittecar, pp. 119–130, Geol. Soc. of Am., Boulder, Colo., doi:10.1130/2009.2451(08).
Gran, K. B., P. Belmont, S. Day, C. Jennings, J. W. Lauer, E. Viparelli, P. Wilcock, and G. Parker (2011), An integrated sediment budget for the Le Sueur River Basin, *Rep. wq-iw7-29o*, 128 p., Minn. Pollut. Control Agency, Mankato. [Available at http://www.pca.state.mn.us/index.php/view-document.html?gid=16202, last accessed 17 May 2016.]
Hansen, A. T., J. A. Czuba, J. Schwenk, A. Longjas, M. Danesh-Yazdi, D. J. Hornbach, and E. Foufoula-Georgiou (2016), Coupling freshwater mussel ecology and river dynamics using a simplified dynamic interaction model, *Freshwater Sci.*, *35*(1), 200–215, doi:10.1086/684223.
Horizon Systems (2014), NHDPlus Version 2, Horizon Systems Corporation, Herndon, Va. [Available at http://www.horizon-systems.com/NHDPlus/NHDPlusV2_home.php, last accessed 1 April 2016.]
Istanbulluoglu, E., D. G. Tarboton, R. T. Pack, and C. H. Luce (2004), Modeling of the interactions between forest vegetation, disturbances, and sediment yields, *J. Geophys. Res.*, *109*, F01009, doi:10.1029/2003JF000041.

Jacobson, R. B., and K. B. Gran (1999), Gravel sediment routing from widespread, low- intensity landscape disturbance, Current River Basin, Missouri, *Earth Surf. Process. Landforms*, *24*(10), 897–917, doi:10.1002/(SICI)1096-9837(199909)24:10<897::AID-ESP18>3.0.CO;2-6.

James, L. A. (2010), Secular sediment waves, channel bed waves, and legacy sediment, *Geogr. Compass*, *4*(6), 576–598, doi:10.1111/j.1749-8198.2010.00324.x.

Jin, S., L. Yang, P. Danielson, C. Homer, J. Fry, and G. Xian (2013), A comprehensive change detection method for updating the National Land Cover Database to circa 2011, *Remote Sens. Environ.*, *132*, 159–175, doi:10.1016/j.rse.2013.01.012.

Jerolmack, D. J., and C. Paola (2010), Shredding of environmental signals by sediment transport, *Geophys. Res. Lett.*, *37*, L19401, doi:10.1029/2010GL044638.

Kelley, D. W., and E. A. Nater (2000), Historical sediment flux from three watersheds into Lake Pepin, Minnesota, USA, *J. Environ. Qual.*, *29*, 561–568, doi:10.2134/jeq2000.00472425002900020025x.

Keulegan, G. H. (1938), Laws of turbulent flow in open channels, *J. Nat. Bureau Standards*, Research Paper 1151, *21*, 707–741.

Kirsch, N. A., S. A. Hanson, P. A. Renard, and J. W. Enblom (1985), Biological survey of the Minnesota River, Minnesota Dept. of Natural Resources Fisheries, Special Publication 139, St. Paul, Minn., 85 p. [Available at http://files.dnr.state.mn.us/publications/fisheries/special_reports/139.pdf, last accessed 22 April 2016.]

Kronvang, B., H. E. Andersen, S. E. Larsen, and J. Audet (2013), Importance of bank erosion for sediment input, storage and export at the catchment scale, *J. Soils Sediments*, *13*, 230–241, doi:10.1007/s11368-012-0597-7.

Lauer, J. W., and J. Willenbring (2010), Steady state reach-scale theory for radioactive tracer concentration in a simple channel/floodplain system, *J. Geophys. Res.*, *115*, F04018, doi:10.1029/2009JF001480.

Lauer, J. W., E. Viparelli, and H. Piégay (2016), Morphodynamics and sediment tracers in 1-D (MAST-1D): 1-D sediment transport that includes exchange with an off-channel sediment reservoir, *Adv. Water Resour.*, doi:10.1016/j.advwatres.2016.01.012.

Lenhart, C. F., M. L. Titov, J. S. Ulrich, J. L. Nieber, and B. J. Suppes (2013), The role of hydrologic alteration and riparian vegetation dynamics in channel evolution along the lower Minnesota River, *Trans. Am. Soc. Agric. Biol. Eng.*, *56*(2), 549–561, doi:10.13031/2013.42686.

Lisle, T. E. (2008), The evolution of sediment waves influenced by varying transport capacity in heterogeneous rivers, in *Gravel-Bed Rivers VI: From Process Understanding to River Restoration*, edited by H. Habersack, H. Piegay, M. Rinaldi, pp. 443–469, Elsevier, Amsterdam, Netherlands, doi:10.1016/S0928-2025(07)11136-6.

Malmon, D. V., T. Dunne, and S. L. Reneau (2003), Stochastic theory of particle trajectories through alluvial valley floors, *J. Geol.*, *111*, 525–542.

Massoudieh, A., A. Gellis, W. S. Banks, and M. E. Wieczorek (2013), Suspended sediment source apportionment in Chesapeake Bay watershed using Bayesian chemical mass balance receptor modeling, *Hydrol. Process.*, *27*, 3363–3374, doi:10.1002/hyp.9429.

McKay, L., et al. (2012), NHDPlus Version 2: User Guide, U.S. Environmental Protection Agency, Washington, D. C. [Available at (ftp://ftp.horizon-systems.com/NHDPlus/NHDPlusV21/Documentation/NHDPlusV2_User_Guide.pdf), last accessed 1 April 2016.]

Minnesota Pollution Control Agency (2014), General report to the congress of the United States pursuant to section 305(b) of the 1972 clean water act: Water years 2012-2013, Minnesota Pollution Control Agency Report wq-s7-50, 62 p., St. Paul, Minn. [Available at https://www.pca.state.mn.us/water/water-quality-assessment-and-listing, last accessed 26 April 2016.]

Musser, K., S. Kudelka, and R. Moore (2009), Minnesota River Basin trends, Water Resources Center Report, Minnesota State University, Mankato, Minn., 64 p.

Muzikar, P. (2008), Cosmogenic nuclide concentrations in episodically eroding surfaces: Theoretical results, *Geomorphology*, *97*(3–4), 407–413, doi:10.1016/j.geomorph.2007.08.020.

Neal, C. W. M., and A. M. Anders (2015), Suspended sediment supply dominated by bank erosion in a low-gradient agricultural watershed, Wildcat Slough, Fisher, Illinois, United States, *J. Soil Water Conserv.*, *70*(3), 145–155, doi:10.2489/jswc.70.3.145.

Novotny, E. V., and H. G. Stefan (2007), Stream flow in Minnesota: Indicator of climate change, *J. Hydrol.*, *334*(3–4), 319–333, doi:10.1016/j.jhydrol.2006.10.011.

Ojakangas, R. W., and C. L. Matsch (1982), *Minnesota's Geology*, p. 255, Univ. of Minn. Press, Minneapolis, Minn.

Paola, C., P. L. Hellert, and C. L. Angevine (1992), The large-scale dynamics of grain-size variation in alluvial basins, 1: Theory, *Basin Res.*, *4*(2), 73–90, doi:10.1111/j.1365-2117.1992.tb00145.x.

Parker, G. (2004), 1D sediment transport Morphodynamics with applications to rivers and turbidity currents, Urbana, Ill. [Available at http://hydrolab.illinois.edu/people/parkerg//morphodynamics_e-book.htm, last accessed 14 November 2016].

Parker, G. (2008), Transport of gravel and sediment mixtures, in *Sedimentation Engineering: Processes, Measurements, Modeling, and Practice: ASCE Manuals and Reports on Engineering Practice*, vol. 110, edited by M. H. Garcia, pp. 165–251, ASCE, Reston, Virginia.

Passalacqua, P., P. Tarolli, and E. Foufoula-Georgiou (2010), Testing space-scale methodologies for automatic geomorphic feature extraction from lidar in a complex mountainous landscape, *Water Resour. Res.*, *46*, W11535, doi:10.1029/2009WR008812.

Passalacqua, P., P. Belmont, and E. Foufoula-Georgiou (2012), Automatic geomorphic feature extraction from lidar in flat and engineered landscapes, *Water Resour. Res.*, *48*, W03528, doi:10.1029/2011WR010958.

Passalacqua, P., et al. (2015), Analyzing high resolution topography for advancing the understanding of mass and energy transfer through landscapes: A review, *Earth-Sci. Rev.*, *148*, 174–193, doi:10.1016/j.earscirev.2015.05.012.

Pizzuto, J. E. (2012), Predicting the accumulation of mercury-contaminated sediment on riverbanks—An analytical approach, *Water Resour. Res.*, *48*, W07518, doi:10.1029/2012WR011906.

Pizzuto, J., et al. (2014), Characteristic length scales and time-averaged transport velocities of suspended sediment in the mid-Atlantic region, U.S.A, *Water Resour. Res.*, *50*, 790–805, doi:10.1002/2013WR014485.

Renard, K. G., G. R. Foster, G. A. Weesies, D. K. McCool, and D. C. Yoder (1997), *Predicting Soil Erosion by Water: A Guide to Conservation Planning With the Revised Universal Soil Loss Equation (RUSLE)*, vol. 703, p. 407, United States Dep. of Agriculture, Washington, D. C.

Rinaldo, A., P. Benettin, C. J. Harman, M. Hrachowitz, K. J. McGuire, Y. van der Velde, E. Bertuzzo, and G. Botter (2015), Storage selection functions: A coherent framework for quantifying how catchments store and release water and solutes, *Water Resour. Res.*, *51*, 4840–4847, doi:10.1002/2015WR017273.

Rodriguez-Iturbe, I., and P. S. Eagleson (1987), Mathematical models of rainstorm events in space and time, *Water Resour. Res.*, *23*(1), 181–190, doi:10.1029/WR023i001p00181.

Schaffrath, K. R., P. Belmont, and J. M. Wheaton (2015), Landscape-scale geomorphic change detection: Quantifying spatially variable uncertainty and circumventing legacy data issues, *Geomorphology*, *250*, 334–348, doi:10.1016/j.geomorph.2015.09.020.

Schmitt, R. J. P., S. Bizzi, and A. Castelletti (2016), Tracking multiple sediment cascades at the river network scale identifies controls and emerging patterns of sediment connectivity, *Water Resour. Res.*, *52*, 3941–3965, doi:10.1002/2015WR018097.

Schottler, S. P., J. Ulrich, P. Belmont, R. Moore, J. W. Lauer, D. R. Engstrom, and J. E. Almendinger (2014), Twentieth century agricultural drainage creates more erosive rivers, *Hydrol. Process.*, *28*(4), 1951–1961, doi:10.1002/hyp.9738.

Shenk, G. W., and L. C. Linker (2013), Development and application of the 2010 Chesapeake Bay watershed total maximum daily load model, *J. Am. Water Resour. Assoc.*, *49*(5), 1042–1056, doi:10.1111/jawr/12109.

Singh, A., E. Foufoula-Georgiou, F. Porté-Agel, and P. R. Wilcock (2012), Coupled dynamics of the co-evolution of gravel bed topography, flow turbulence and sediment transport in an experimental channel, *J. Geophys. Res.*, *117*, F04016, doi:10.1029/2011JF002323.

Singh, A., F. Porté-Agel, and E. Foufoula-Georgiou (2010), On the influence of gravel bed dynamics on velocity power spectra, *Water Resour. Res.*, *46*, W04509, doi:10.1029/2009WR008190.

STATSGO2 (2015), *Description of the STATSGO2 Database*, Natural Resources Conservation Service, Washington, D. C. [Available at http://www.nrcs.usda.gov/wps/portal/nrcs/detail/soils/survey/geo/?cid=nrcs142p2_053629, last accessed 4 August 2015].

Stout, J. C., P. Belmont, S. P. Schottler, and J. K. Willenbring (2014), Identifying sediment sources and sinks in the Root River, southeastern Minnesota, *Ann. Assoc. Am. Geogr.*, *104*(1), 20–39, doi:10.1080/00045608.2013.843434.

Tarboton, D. G., R. L. Bras, and I. Rodriguez-Iturbe (1991), On the extraction of channel networks from digital elevation data, *Hydrol. Process.*, *5*(1), 81–100, doi:10.1002/hyp.3360050107.

Trimble, S. W. (1981), Changes in sediment storage in the Coon Creek basin, Driftless Area, Wisconsin, 1853 to 1975, *Science*, *214*(4517), 181–183, doi:10.1126/science.214.4517.181.

Trimble, S. W. (1983), A sediment budget for Coon Creek basin in the Driftless Area, Wisconsin, 1853-1977, *Am. J. Sci.*, *283*(5), 454–474, doi:10.2475/ajs.283.5.454.

Tucker, G. E., and R. L. Bras (2000), A stochastic approach to modeling the role of rainfall variability in drainage basin evolution, *Water Resour. Res.*, *36*(7), 1953–1964, doi:10.1029/2000WR900065.

U.S. Geological Survey (2014), USGS water data for Minnesota, U.S. Geol. Surv., Reston, Va. [Available at http://waterdata.usgs.gov/mn/nwis?, last accessed 20 May 2014].

Van De Wiel, M. J., and T. J. Coulthard (2010), Self-organized criticality in river basins: Challenging sedimentary records of environmental change, *Geology*, *38*(1), 87–90, doi:10.1130/G30490.1.

Vanoni, V. A. (1975), *Sedimentation Engineering*, vol. 54, p. 726, American Society of Engineers Manuals and Reports on Engineering Practice, Reston, Va.

Viparelli, E., J. W. Lauer, P. Belmont, and G. Parker (2013), A numerical model to develop long-term sediment budgets using isotopic sediment fingerprints, *Comput. Geosci.*, *53*, 114–122, doi:10.1016/j.cageo.2011.10.003.

Wilkinson, S. N., I. P. Prosser, and A. O. Hughes (2006), Predicting the distribution of bed material accumulation using river network sediment budgets, *Water Resour. Res.*, *42*, W10419, doi:10.1029/2006WR004958.

Wu, W., and S. Wang (2006), Formulas for sediment porosity and settling velocity, *J. Hydraul. Eng.*, *132*, 858–862, doi:10.1061/(ASCE)0733-9429(2006)132:8(858).

Yang, M.-S., and K. T. Lee (2001), Determination of probability distributions for Strahler stream lengths based on Poisson process and DEM, *Hydrol. Sci. J.*, *46*(5), 813–824, doi:10.1080/02626660109492872.